AGU PUBLICATIONS

JGR

Journal of Geophysical Research: Oceans

RESEARCH ARTICLE

10.1002/2015JC011145

A comparative assessment of coastal mean dynamic topography in Norway by geodetic and ocean approaches

Vegard Ophaug[1], Kristian Breili[1,2], and Christian Gerlach[1,3]

[1]Department of Mathematical Sciences and Technology, Norwegian University of Life Sciences (NMBU), Ås, Norway, [2]Geodetic Institute, Norwegian Mapping Authority, Hønefoss, Norway, [3]Commission of Geodesy and Glaciology, Bavarian Academy of Sciences and Humanities, Munich, Germany

Key Points:
- First comprehensive validation of coastal MDT by geodetic and ocean approaches in Norway
- Along the Norwegian coast, geodetic and ocean MDTs agree on the 3–11 cm level
- Dedicated coastal altimetry products generally do not offer improvements over conventional products

Supporting Information:
- Supporting Information S1
- Supporting Information S2
- Supporting Information S3

Correspondence to:
V. Ophaug,
vegard.ophaug@nmbu.no

Citation:
Ophaug, V., K. Breili, and C. Gerlach (2015), A comparative assessment of coastal mean dynamic topography in Norway by geodetic and ocean approaches, *J. Geophys. Res. Oceans*, *120*, 7807–7826, doi:10.1002/2015JC011145.

Received 15 JUL 2015
Accepted 3 NOV 2015
Accepted article online 5 NOV 2015
Published online 12 DEC 2015

Abstract The ocean's mean dynamic topography (MDT) is the surface representation of ocean circulation. It may be determined by the ocean approach, using numerical ocean circulation models, or by the geodetic approach, where MDT is the height of the mean sea surface (MSS), or mean sea level (MSL), above the geoid. Using new geoid models, geodetic MDT profiles based on tide gauges, dedicated coastal altimetry products, and conventional altimetry are compared with six ocean MDT estimates independent of geodetic data. Emphasis is put on the determination of high-resolution geoid models, combining ESA's fifth release (R5) of GOCE satellite-only global gravity models (GGMs) with a regional geoid model for Norway by a filtering technique. Differences between MDT profiles along the Norwegian coast together with Taylor diagrams confirm that geodetic and ocean MDTs agree on the ∼3–7 cm level at the tide gauges, and on the ∼5–11 cm level at the altimetry sites. Some geodetic MDTs correlate more with the best-performing ocean MDT than do other ocean MDTs, suggesting a convergence of the methods. While the GOCE R5 geoids are shown to be more accurate over land, they do not necessarily show the best agreement over the ocean. Pointwise monomission altimetry products give results comparable with the multimission DTU13MSS grid on the ∼5 cm level. However, dedicated coastal altimetry products generally do not offer an improvement over conventional altimetry along the Norwegian coast.

1. Introduction

The mean dynamic topography (MDT) is the height of the time-mean sea surface above the geoid. Its slope reveals the magnitude and direction of ocean surface geostrophic currents; hence, it is a surface representation of the ocean's mean circulation. Historically, oceanographers have determined the global ocean circulation by means of hydrographic measurements of temperature and salinity (in situ data) from ships [*Pugh and Woodworth*, 2014]. Today, the oceanographic MDT is determined from numerical ocean models, which employ a set of dynamical equations and are driven by in situ data sets, meteorological wind and air pressure information, and hydrological information. This may be termed the *ocean approach* to MDT computation.

A precise geoid model in combination with observations of the mean sea surface (MSS) by means of satellite altimetry allows a *geodetic approach* to determine the MDT. Altimetric observations yield ellipsoidal heights of the MSS. With geoid heights above the same ellipsoid, the MDT may be derived through a purely geometrical approach based on geodetic observations. The same principle can be applied if ellipsoidal heights of mean sea level (MSL), as observed by tide gauges connected to a geodetic reference frame, are available.

The rapid development of geodetic measurement techniques and models has rendered them sufficiently accurate to complement and validate traditional oceanographic results. The European Space Agency (ESA) gravimetric satellite mission Gravity and steady-state Ocean Circulation Explorer (GOCE) [*Drinkwater et al.*, 2003] provides a global geoid with unprecedented detail and has significantly improved geodetic MDT determination. Presently, ocean and geodetic MDTs show an average agreement on subdecimetric level, with better agreement in the open ocean than along coastlines [e.g., *Bingham et al.*, 2011; *Albertella et al.*, 2012; *Griesel et al.*, 2012; *Johannessen et al.*, 2014; *Higginson et al.*, 2015; *Hughes et al.*, 2015; *Woodworth et al.*, 2015].

The circulation of the Norwegian Sea incorporates a poleward transport of warm surface water from the North Atlantic Ocean (Norwegian Atlantic Current) as well as the Baltic Sea (Norwegian Coastal Current), with implications for the Norwegian coastal ecosystem [e.g., *Mork and Skagseth*, 2010; *Skagseth et al*., 2011]. This heat transport maintains a relatively mild climate in northwest Europe, as well as North Atlantic Deep Water formation, sustaining the Atlantic Meridional Overturning Circulation [*Rhines et al*., 2008]. Consequently, a quantitative understanding of ocean circulation variability at northern high latitudes is crucial to environmental and climate-related studies.

Coastal ocean dynamics has gained recent interest due to its importance for shipping, fishery, coastal ecosystem processes, other on-shore and offshore activities, and sea-level rise [*Pugh and Woodworth*, 2014]. In geodesy, coastal MDT remains an important implement for height system unification, wherein a precise geoid represents the reference surface for heights [*Rummel*, 2012]. However, the coastal zone presents a multitude of challenges regarding geoid and MDT computation. Both geodetic and ocean approaches to MDT computation show irregularities close to the coast [e.g., *Woodworth et al*., 2012; *Featherstone and Filmer*, 2012; *Filmer*, 2014]. Land contaminates coastal altimetry observations [e.g., *Gommenginger et al*., 2011] and tide-gauge observations are affected by vertical land motion [e.g., *Pugh and Woodworth*, 2014]. Tides become more complex along the coast, and global tide models loose validity there [e.g., *Ray et al*., 2011]. It is generally challenging to make observations from land, open sea, and coast consistent with each other [e.g., *Woodworth et al*., 2012]. Only a few numerical ocean models and selected coastal altimetry products have been developed for pilot studies or for specific areas. The Norwegian coast adds further complications, due to the many islands, mountains, and deep, narrow fjords.

A thorough validation of the quality of coastal products, specifically for the Norwegian coast, does not exist. The main goal of this work is to explore the level of agreement between novel geodetic and recent ocean MDT estimates along the Norwegian coast. A secondary goal is to assess whether geodetic MDTs using new GOCE geoid models offer an improvement over existing models. Finally, we investigate whether two dedicated coastal altimetry products perform better than the pure altimetry observations they are based on, and how pointwise altimetry compares with a state-of-the-art global gridded altimetry product.

Three fundamental vertical reference surfaces (or vertical datums) are considered in geodesy: the reference ellipsoid, the geoid, and the quasigeoid. While the reference ellipsoid is a vertical reference for nonphysical heights, the geoid and quasigeoid are vertical references for physical heights (orthometric and normal heights, respectively), incorporating gravity. The distinction between the geoid and the quasigeoid is not important in this work, as the geoid and the quasigeoid coincide over the oceans, with assumed negligible differences at the coast. However, all geoid models in this work are strictly quasigeoids, in the form of quasigeoid heights (better known as *height anomalies* in geodesy).

Geodetic MDTs have been determined using four quasigeoid models (see Table 6), two of which have been determined specifically for this work by a filtering approach, combining a regional quasigeoid model for Norway with the fifth release (R5) of ESA's GOCE satellite-only global gravity models (GGMs). The remaining two are the original Norwegian regional quasigeoid model and a quasigeoid model based on the GGM EGM2008.

Both tide-gauge and altimetry observations have been employed in this work. We aim to compare coastal geodetic MDTs based on these different observational methods. We have selected six ocean MDTs independent of geodetic data, primarily for validating our geodetic MDTs, but also to reveal their consistency along the coast. Section 2 describes the data sets in detail, with focus on data consistency. In section 3, we make a comparison of geodetic and ocean MDTs, before discussing the results in section 4. Conclusions are presented in section 5.

2. Data and Methods

2.1. Geodetic Approach

2.1.1. Regional Quasigeoids Based on GOCE

We investigate the performance of regional quasigeoids based on GOCE R5 GGMs, specifically the TIM5 and DIR5 models, based on the time-wise [*Brockmann et al*., 2014] and direct [*Bruinsma et al*., 2013] approaches,

Table 1. Validation of Best Combined and Pure Quasigeoid Models

Quasigeoid Model	$\hat{\sigma}$ (cm)
TIM5 + NMA2014 filtered @ 80 km	3.07
DIR5 + NMA2014 filtered @ 80 km	3.07
NMA2014	3.49
EGM2008[a]	4.64
GOCE TIM5[b]	28.23
GOCE DIR5[b]	27.37

[a]Developed to d/o 2190.
[b]Developed to d/o 280 (TIM5) and 300 (DIR5), and including omission errors.

respectively. These GGMs are given as sets of spherical harmonic coefficients to degree and order (d/o) 280 (TIM5) and 300 (DIR5), thus limited to a spatial resolution of ∼80–100 km, and with an accuracy of ∼1–4 cm (at d/o 220) [*Gruber*, 2014]. As the smallest spatial scales of the gravity field are not resolved, an omission error of ∼30 cm is introduced, if the GGMs are used alone [e.g., *Haines et al*., 2011]. This is demonstrated in Table 1, described below. Such an omission error is not negligible for our detailed studies of MDT along the Norwegian coast. Computing a regional gravimetric quasigeoid using the new GGMs in combination with terrestrial gravity data would be the optimal solution to this problem; this, however, is a time-consuming and computationally intensive task outside the scope of this work.

Instead, we have increased the resolution of the GGMs by combining them with the latest regional quasigeoid model for Norway, NMA2014, provided by the Norwegian Mapping Authority (NMA) (O. C. D. Omang, personal communication, 2014). It is based on the remove-compute-restore method [e.g., *Denker*, 2013], and the Wong and Gore kernel modification of Stokes's formula [*Wong and Gore*, 1969], evaluated by the 2-D multiband spherical FFT method [e.g., *Sideris*, 2013]. The DIR4 GGM was used as a global reference model. The Wong and Gore degree of modification is 140, with a linear transition from degree 130 to 140 to reduce edge effects, reflecting the best agreement in comparison with GNSS/leveling based on trial runs [e.g., *Forsberg and Featherstone*, 1998; *Omang and Forsberg*, 2002]. Consequently, above d/o 140, NMA2014 is solely based on terrestrial data. Bearing in mind that GOCE delivers accuracy improvements mainly in the medium wavelengths between d/o 100 and 200 in Norway [e.g., *Šprlák et al*., 2015], we expect an improvement in the accuracy of our combined quasigeoid model.

As NMA2014 is given on a regular grid with $0.01^\circ \times 0.02^\circ$ spacing, within an area delimited by $53^\circ \leq \varphi \leq 77.99^\circ$, and $-15^\circ \leq \lambda \leq 40^\circ$, GOCE TIM5 and DIR5 height anomalies have been computed on the NMA2014 grid points by spherical harmonic synthesis (SHS). Height anomalies are defined as $\zeta = T/\gamma$ [*Hofmann-Wellenhof and Moritz*, 2005, equation (8–26)], where T is the disturbing potential on Earth's surface, and γ is the normal gravity acceleration on the telluroid (an approximation of Earth's surface). Naturally, we have neither ellipsoidal nor normal heights for each NMA2014 grid point; instead, we have used topographic heights (excluding bathymetry) from the global ACE2 $30'' \times 30''$ digital elevation model [*Berry et al*., 2010], bilinearly interpolated to the NMA2014 grid points. ACE2 topographic heights are a fusion of orthometric height data from the Shuttle Radar Topography Mission (SRTM) and altimetry (ERS-1, ERS-2, and Envisat). For our purposes, these heights are assumed to be a sufficient approximation to normal heights. The effect of this approximation was investigated by initially computing height anomalies using topographic heights from ACE2, then adding them to the topographic heights, yielding approximated ellipsoidal heights, before finally computing height anomalies using both approximated normal and ellipsoidal heights. The difference between computed height anomalies using the simple approach (based on approximated normal heights only), and the more rigorous two-step approach (based on both approximated normal and ellipsoidal heights), was found to be insignificant at the mm level. Therefore, we used the simple approach for quasigeoid computation by SHS. Finally, we also considered the GGM EGM2008 [*Pavlis et al*., 2012], given as a set of spherical harmonic coefficients to d/o 2190, corresponding to a spatial resolution of 5 arc min. The EGM2008 quasigeoid was computed by SHS to its maximum d/o in the same manner as the TIM5 and DIR5 GGMs (Table 1).

Closely following the approach of *Rülke et al*. [2012], the TIM5 and DIR5 quasigeoids were low-pass filtered using the Gaussian mean kernel [*Jekeli*, 1981, equation (61)], and NMA2014 high-pass filtered with the complementary filter. Filtering was done by a convolution in the spatial domain, evaluated by the 1D-FFT method of *Haagmans et al*. [1993]. We used an integration radius of 4°, ensuring filter weights close to zero at the domain edges. Ultimately, the filtered quasigeoids were added, giving combined quasigeoids TIM5+NMA2014 and DIR5+NMA2014, delimited by $57^\circ \leq \varphi \leq 73.99^\circ$ and $-11^\circ \leq \lambda \leq 36^\circ$. Eight filter-combined solutions were computed for filter radii between 40 and 110 km at 10 km intervals, and validated externally by comparison with observed height anomalies, determined at sites observed both by GNSS and

Table 2. Tide Gauges in Our Work

Tide Gauge	Code	φ (°)	λ (°)
Vardø	VARD	70.375	31.104
Honningsvåg	HONN	70.980	25.973
Hammerfest	HAMM	70.665	23.683
Tromsø	TROM	69.647	18.961
Andenes	ANDE	69.326	16.135
Harstad	HARS	68.801	16.548
Kabelvåg	KABE	68.213	14.482
Bodø	BODO	67.288	14.391
Rørvik	RORV	64.860	11.230
Mausund[a]	MAUS	63.869	8.666
Heimsjø	HEIM	63.425	9.102
Kristiansund	KRIN	63.114	7.734
Ålesund	ALES	62.469	6.152
Måløy	MALO	61.934	5.113
Bergen	BERG	60.398	5.321
Stavanger	STAV	58.974	5.730
Tregde	TREG	58.006	7.555
Helgeroa	HELG	58.995	9.856
Viker	VIKE	59.036	10.950

[a]Mausund is not part of the PSMSL database.

leveling. For this, we have used a set of 1344 GNSS/leveling points in Norway, provided by NMA (Omang, personal communication, 2014). We acknowledge that the Gaussian kernel is a basic way of weighting terrestrial and satellite data, because it does not take data quality into account. Better results may be obtained using a stochastic kernel, weighting the data more correctly.

Table 1 shows validation results from pure and combined quasigeoids, in the form of standard deviations of differences between modeled and observed height anomalies. A greater filter radius means that more of the regional quasigeoid is incorporated into the combined model. We found an optimum filter radius of 80 km for both TIM5+NMA2014 and DIR5+NMA2014, where the combined quasigeoids perform better than NMA2014. In addition to the four high-resolution quasigeoids used in this work, the pure GOCE DIR5 and TIM5 model results are shown in Table 1, to quantify the omission error.

All height anomalies in this work refer to the GRS80 ellipsoid, with a semimajor axis of 6,378,137 m and an inverse flattening of 1/298.2572 (and practically equal to the WGS84 ellipsoid). With regard to the treatment of the permanent tides, we have decided to standardize all our data sets in the mean tide (MT) system, which retains the permanent tide effects from external bodies (mainly the Sun and the Moon). As the quasigeoids are given in the conventional tide free system (TF, where direct and indirect effects of the Sun and the Moon are removed), they were converted to the MT system using *Ekman* [1989, equation (17)].

Jayne [2006] as well as *Woodworth et al.* [2015] underline the importance of not mixing altimetry-derived gravity information in a quasigeoid model for MDT estimation purposes, as some of the dynamic topography will blend into the quasigeoid model, corrupting the MDT estimate when combined with the ocean's time-mean surface from altimetry or tide gauges. In this respect, there is a considerable difference between NMA2014 and EGM2008. EGM2008 incorporates a $5' \times 5'$ gravity anomaly data set, which relies heavily on altimetry-derived gravity information over the oceans. Only a small amount of altimetry-derived gravity data are included in NMA2014, in areas sparsely covered with shipborne and airborne gravity data, more than $\sim$500 km off the Norwegian coast (Omang, personal communication, 2014). Therefore, we regard NMA2014 as a purely gravimetric quasigeoid for our purposes. The distributions of terrestrial and altimetry-derived gravity data in NMA2014 are provided in supporting information Figures S1 and S2.

2.1.2. Tide-Gauge MSL

The Norwegian tide-gauge network comprises 24 tide gauges. Not all have been considered in our work. We have omitted the tide gauge in Ny-Ålesund due to its location on the Svalbard archipelago in the Arctic Ocean, outside our study area. Also, we have not considered the tide gauges in Oslo, Oscarsborg, Trondheim, and Narvik, located well inside fjords not covered by the coastal altimetry data. At these tide gauges, complex local dynamics not resolved by the ocean models are expected to considerably contribute to observed MSL, thus unnecessarily complicating our comparative assessment. Consequently, we have included MSL observations from 19 tide gauges along the Norwegian coast (Table 2 and Figure 1), averaged over the epoch 1996–2000 inclusive, so as to be in the same epoch as the ocean models.

With the exception of the tide gauge in Mausund, we have used annual values of MSL from the Permanent Service for Mean Sea Level (PSMSL) [*Holgate et al.*, 2013] at http://www.psmsl.org/data/obtaining/. Mausund was recently transferred to the official Norwegian tide-gauge network, which is maintained by NMA. Mausund data are not yet available at PSMSL, but its inclusion is planned (A. Voldsund, NMA, personal communication, 2015). In this work, we have used hourly MSL values for Mausund from the NMA database, averaged to monthly values. These values are given in the former national height system, NN1954.

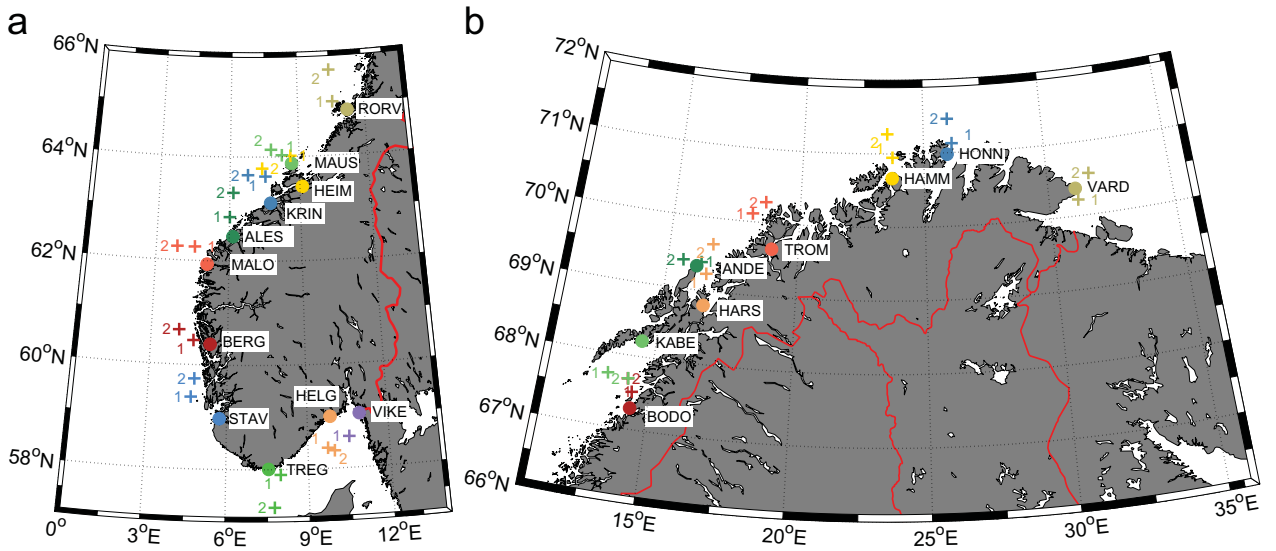

Figure 1. Tide-gauge MSL (dots) and altimetric MSS (plus signs) (a) south of 66°N and (b) north of 66°N.

Horizontal tide-gauge coordinates have been obtained using the tide and sea level web service of the NMA at http://www.kartverket.no/en/sehavniva/(with an uncertainty of ∼30 m) and have been compared with the cruder ones at PSMSL (with an uncertainty of ∼100 m), discovering no significant difference.

All PSMSL data in this work are within the Revised Local Reference (RLR) data subset, meaning that MSL is given relative to a tide-gauge benchmark (TGBM) at each tide gauge. Ideally, the absolute height of MSL should be determined directly by Global Navigation Satellite Systems (GNSS), either continuously or by precise campaign measurements at the tide gauge itself or a nearby benchmark with a leveled connection to a TGBM. By these approaches, the vertical uncertainty is within ∼1–2 cm [*Rothacher*, 2002].

Unfortunately, none of the TGBMs in our work have been observed by GNSS with sufficient accuracy. Some of the tide gauges have GNSS receivers mounted on them, but lack the necessary connection between the antenna reference point and the tide gauge zero, because they were installed with the aim of monitoring relative vertical site displacements only.

A solution for the interim is to derive ellipsoidal heights of MSL by using a height reference conversion surface (HRCS). This surface is typically a geoid fitted to benchmarks with known heights both in the national height system by means of leveling, and ellipsoidal heights h observed by GNSS, enabling the conversion of heights H in the national height system into ellipsoidal ones by the simple relation:

$$h = H + \mathrm{HRCS}. \tag{1}$$

We have used the Norwegian height reference surface HREF [*Solheim*, 2000], necessarily aggravating the total error budget due to possible errors in the quasigeoid on which the conversion surface is based, errors from GNSS/leveling benchmark interpolation, as well as errors in the national leveling network [*Featherstone*, 2008]. *Mysen* [2014] derived a formal HREF uncertainty map using least squares collocation, covering Norway south of 65°N, with coastal uncertainties ranging from ∼1 to ∼3 cm. Although they conclude that these uncertainties may be too optimistic, and uncertainties for Northern Norway have yet to be estimated, we reckon these as best present estimates for error budgeting purposes.

Currently, Norway is in the process of changing its height system. The former spheroidal-orthometric height system of Norway, NN1954, refers to a benchmark close to the tide gauge in Tregde, and was based on an adjustment of MSL determined at seven tide gauges along the coast [*Lysaker et al.*, 2007]. The new normal height system, NN2000, refers to the Normaal Amsterdams Peil, and is based on a common Nordic adjustment with reference epoch 2000.0, taking vertical land motion [*Vestøl*, 2006; *Ågren and Svensson*, 2007] into account. Further deviations of NN2000 from NN1954 are due to different treatment of the permanent tides, which will be discussed below. *Featherstone and Filmer* [2012] showed that a tilt in the Australian Height

Datum, a height system established in a similar manner as NN1954, constrained to MSL at multiple tide gauges, was almost completely due to neglecting MDT effects at these tide gauges. NN2000, on the other hand, should be free of any MDT effects. In order to explore whether possible artifacts in the height systems significantly affect final MDT estimates, tide-gauge MSL was computed using both the former NN1954-constrained conversion surface HREF2008a, as well as the current NN2000-constrained conversion surface HREF2014c.

For all tide gauges except Mausund, the ellipsoidal heights of the TGBMs were computed according to equation (1) (using either NN1954-related or NN2000-related quantities H and HRCS). Next, the ellipsoidal height of MSL was computed by subtracting the height difference between TGBM and MSL (given by the RLR) from the ellipsoidal height of the TGBM.

For Mausund, the ellipsoidal height of MSL could be computed without going via the TGBM, using equation (1) as well as NN1954-related quantities H and HRCS. The height of MSL in NN1954 was transferred to NN2000 by forming a height difference between NN1954 and NN2000 at Mausund TGBM, and adding it to MSL.

The standard deviation of the differences between derived ellipsoidal heights of MSL using either NN1954 heights with HREF2008a or NN2000 heights with HREF2014c, amounts to 2.8 cm, with discrepancies ranging from -7.9 cm (Andenes) to 4.4 cm (Hammerfest) (Figure 2d).

HREF is derived from ellipsoidal heights given in the TF system. Therefore, ellipsoidal heights of MSL derived from HREF are also given in the TF system, and we converted them to the MT system using *Petit and Luzum* [2010, equation (7.14a)]. This latitude-dependent conversion ranges from ~-7 cm in Southern Norway, to ~-10 cm in Northern Norway. The ellipsoidal heights of MSL refer to the GRS80 ellipsoid.

MSL was corrected for the ocean's inverted barometer (IB) response (static atmospheric loading effect) using *Wunsch and Stammer* [1997, equation (1)], and local monthly sea level pressure data obtained from the eKlima database of the Norwegian Meteorological Institute at http://eklima.met.no, with respect to a reference value of 1011.4 mbar [*Woodworth et al*., 2012]. The mean distance between tide gauge and pressure data sites is $\sim$16 km, and the IB correction ranges from -47 to $+4$ mm.

Furthermore, a correction for the nodal tide, a long-period (18.61 years) astronomical tide, was applied to the MSL values using *Woodworth* [2012, equation (1), scaled by 0.44 according to *Pugh and Woodworth*, 2014]. For our range of latitudes, the nodal tide correction varies between $\sim$7 and $\sim$10 mm.

2.1.3. Altimetric MSS

We have employed six satellite altimetry data sets in this work; two basic monomission Envisat and Jason-2 data sets, three dedicated coastal products based on Envisat and Jason-2, and one multimission gridded product.

Dedicated coastal along-track monomission data have been produced by the Centre de Topographie des Océans et de l'Hydrosphère (CTOH) [*Roblou et al*., 2011], and the Collecte Localisation Satellites (CLS) through the Prototype Innovant de Système de Traitement pour l'Altimétrie Côtière et l'Hydrologie (PISTACH) project [*Mercier et al*., 2008], funded by the Centre National d'Etudes Spaciales (CNES). Both are distributed through the Archivage, Validation et Interprétation de données des Satellites Océanographiques (AVISO) project at http://www.aviso.altimetry.fr.

Processed on a regional basis using the X-TRACK software [*Roblou et al*., 2011], we have used the Envisat CTOH product covering the entire Norwegian coast. It is based on a two-step procedure. First, Geophysical Data Record (GDR) sea surface heights (SSH) have been analyzed applying stricter data validity criteria than normal. If a sudden change in a single range correction term occurs, it implies that the whole altimeter measurement is flagged as erroneous. This first step causes considerable data rejection, which, in a second step, is remedied by data recovery using correction terms interpolated from the valid data. Finally, the SSH values are resampled to reference tracks, producing 1 Hz observations at the same points for each cycle, with $\sim$6 km spacing between the points.

In order to assess whether coastal tuning of Envisat data gives better results along the Norwegian coast, we have also used standard along-track Envisat RA-2 GDR version 2.1 data provided by the European Space Agency (ESA) and downloaded from ESA's Earth Online portal at http://earth.esa.int. Corrections were applied due to an anomaly identified in the flight time delay calibration factor (PTR), estimated as part of the Envisat RA-2 GDR v2.1 reprocessing. The anomalies have a significant effect on mean sea level trend

estimates but are not crucial for the mean sea level itself [*Ollivier and Guibbaud*, 2012]. No PTR corrections are applied in the Envisat CTOH product (CTOH Team, personal communication, 2015). Only the Envisat GDR and CTOH cycles 10–92 were considered, which implies preclusion of the Envisat geodetic mission (cycles 93–113). The Envisat GDR data have a similar along-track spatial resolution as the Envisat CTOH-product (∼6 km), but the observations were not resampled to reference tracks. For the remainder of this work, standard Envisat GDR data will simply be referred to as Envisat, and Envisat CTOH as CTOH.

In addition to the two Envisat-based altimetry products described above, we have considered three products based on Jason-2 observations: one basic Jason-2 product and two PISTACH products. PISTACH is dedicated to the reprocessing of 20 Hz (∼300 m) Jason-2 I-GDR data along coasts and over inland waters, and covers all oceans. Due to the orbit configuration of Jason-2, PISTACH is limited to areas south of 66°N. It employs retracking [*Gommenginger et al*., 2011] schemes, which restrict the analysis window to consider only the coastal waveform gates contaminated by land effects, and filters the waveforms. Again, in order to assess the retracked Jason-2 data, we have used the standard Jason-2 Ku band corrected range measurement with no retracking applied, together with the Red3 and Ocean3 retrackers, dedicated to reduce instrumental noise and improve coastal approach, respectively. Our analysis of the PISTACH data revealed a shift in the sea surface heights around 1 September 2012. Data after this epoch were transformed to the initial mean level by estimating a step function at this epoch by least squares adjustment. We used all Jason-2 PISTACH data available at the time of writing, i.e., cycles 1–228, covering the 2008–2014 period. For the remainder of this work, standard Jason-2 I-GDR data will simply be referred to as Jason-2, and the PISTACH trackers Ocean3 and Red3 will be termed Ocean3 and Red3, respectively.

In general, we have employed standard range and geophysical corrections (ionosphere, troposphere, dynamic atmosphere, sea-state bias, and tides) as provided in the (I-)GDR files. However, there are some exceptions: The wet tropospheric corrections based on radiometer observations have been replaced by ECMWF model corrections within about 50 km of the coastline (which practically includes all MSS sites). In addition, the ionospheric corrections were subject to special attention. For Envisat observations prior to the S-band failure at 17 January 2008, and passing the editing criteria recommended in the Envisat User Manual [*Soussi et al*., 2009], smoothed ionospheric corrections calculated by combining range measurements on the Ku and S bands were used. For other epochs, corrections computed from global ionospheric maps (GIM) were used. We followed a similar approach for the Jason-2 and Ocean3 ranges, while GIMs were used for all Red3 and CTOH ranges. Parametric sea-state bias corrections were applied to all sets of ranges except for Red3, as sea-state bias corrections are presently only available for ocean trackers. For ocean tidal corrections, a mix of models have been used due to different processing standards. The CTOH sea surface heights have been corrected using the FES2012 model, while the FES2004 model was used for the Envisat and Jason-2 data. A third model, GOT4.7, was applied to the Jason-2/PISTACH trackers. Table 3 gives an overview of the applied corrections.

We have chosen 37 MSS sites along the Norwegian coast (Tables 4 and 5 and Figure 1). The MSS sites were chosen using a semiautonomous script, by consecutively plotting each tide gauge and nearby altimetry tracks, and choosing sites where all tracks cross, thus containing observations from all altimetry products. Because only the CTOH data were resampled to reference tracks, we included all sea surface heights within a spherical distance of 5 km from each MSS site (roughly corresponding to an altimetry footprint). To sufficiently represent the Norwegian coast, and also to increase confidence in the MSS observations, we have striven to find two MSS sites per tide gauge fulfilling the above criterion, which was possible for all tide gauges but Viker. The average distances between MSS sites and the coast, and between MSS sites and the associated tide gauges, are 23.1 and 54.1 km, respectively.

To explore whether the chosen MSS sites experience similar temporal variations as the tide gauges, the correlation of the altimetry time series with the associated tide-gauge time series was computed for each MSS site. Also, formal accuracies of the MSS observations were computed from the along-track observation variability. Envisat and CTOH observations have an average standard deviation of ∼1 cm (Tables 4 and 5), with slightly improved numbers south of 66°N (Table 5). On the whole, CTOH presents the lower standard deviation of the two. Observations from Jason-2, Ocean3, and Red3 have an average standard deviation of ∼0.5 cm (Table 5), but here the pure Jason-2 observation accuracy is better than the retrackers. The average correlation of altimetric MSS with tide-gauge MSL is higher north of 66°N, where Envisat on average correlates slightly better (0.74) than CTOH (0.70) (Table 4). Correlation deteriorates for the data south of 66°N, but

Table 3. Applied Range and Geophysical Corrections

Correction	Envisat	CTOH	Jason-2	Ocean3	Red3	DTU13MSS
Dry	ECMWF	ECMWF	ECMWF	ECMWF	ECMWF	ECMWF
Wet	Composite	Radiometer	Composite	Composite	Composite	Radiometer
Iono	IFC+GIM[a]	GIM	IFC+GIM	IFC+GIM	GIM	IFC
LF[b]	IB w/ECMWF	IB w/ECMWF	IB w/ECMWF	IB w/ECMWF	IB w/ECMWF	MOG2D_IB
HF[c]	MOG2D	MOG2D	MOG2D	MOG2D	MOG2D	MOG2D
Sea-State Bias	Non-param	Non-param	Non-param	Non-param	No SSB	Non-param
Ocean Tide	FES2004	FES2012	FES2004	GOT4.7	GOT4.7	GOT4.7
Solid Earth Tide	CT[d]	CT[d]	CT[d]	CT[d]	CT[d]	CT[d]
Pole Tide	*Wahr* [1985]	*Wahr* [1985]	*Wahr* [1985]	*Wahr* [1985]	*Wahr* [1985]	*Wahr* [1985]
Range bias (m)	0.433	0.433	0.174	0.174	0.174	
Cycles	10–92	10–92	1–228	1–228	1–228	
Period	2002–2010	2002–2010	2008–2014	2008–2014	2008–2014	1993–2012

[a]IFC: ionospheric-free combination; GIM: global ionosphere map.
[b]Low-frequency contribution with periods $>$ 20 days.
[c]High-frequency contribution with periods $<$ 20 days.
[d]CT: tidal potential from *Cartwright and Tayler* [1971] and *Cartwright and Edden* [1973].

still Envisat correlates better (0.57) than CTOH (0.53) (Table 5). Jason-2 observations have an average correlation of 0.52, similar to Envisat and CTOH. Furthermore, the Ocean3 and Red3 average correlations (0.39 and 0.32, respectively) are notably lower than the other altimetry data.

Temporal means of observed SSH were formed, where SSH is the difference between the ellipsoidal height of the spacecraft and the observed range between altimeter and sea surface, corrected for atmospheric and sea surface scattering effects as well as tides and atmospheric loading. Consequently, SSH is automatically given in the MT system. In accordance with the standardization of MSL (section 2.1.2), all altimetry observations were first adjusted to the mean epoch (1998.5) of the 1996–2000 period covered by the ocean models (section 2.2). This was done by applying corrections for regional sea level change,

$$\mathrm{SSH}_{1998.5}(t) = \mathrm{SSH}(t) + \beta(1998.5 - t), \tag{2}$$

where $\mathrm{SSH}_{1998.5}(t)$ is the sea surface height observed at epoch t (SSH(t)), transformed back to the mean epoch (1998.5). The local sea level rate (β) was estimated by using records from the associated tide gauges. We have chosen to use tide-gauge records instead of altimetry data because suitable multimission time series are restricted to areas south of 66°N. In addition, regional altimetric sea level rates are quite uncertain (*Prandi et al*. [2012] adopt a total error of 1.3 mm/yr [90% confidence interval] for the Arctic Ocean), especially in the coastal zone. We used monthly tide-gauge records from the PSMSL (see section 2.1.2). Relative sea level rates were estimated by fitting equation (3) to the tide-gauge records by least squares adjustment:

Table 4. MSS Observations From Altimetry North of 66°N (1996–2000)[a]

Site	φ (°)	λ (°)	d_{TG}	d_c	$\hat{\sigma}^{envi}$	$\hat{\sigma}^{ctoh}$	r_{TG}^{envi}	r_{TG}^{ctoh}
$VARD_1$	70.219	31.168	12.9	8.6	1.2	0.9	0.59	0.75
$VARD_2$	70.561	31.711	34.1	28.0	0.9	0.8	0.70	0.60
$HONN_1$	71.127	26.181	17.6	5.2	1.1	1.0	0.73	0.54
$HONN_2$	71.461	26.021	53.3	33.3	0.8	0.8	0.75	0.73
$HAMM_1$	70.948	23.699	31.3	2.9	1.0	0.8	0.80	0.73
$HAMM_2$	71.266	23.481	67.2	26.3	0.7	0.7	0.70	0.60
$TROM_1$	70.280	18.610	71.5	8.4	1.3	1.4	0.70	0.61
$TROM_2$	70.112	18.114	61.1	12.0	0.8	0.8	0.85	0.77
$ANDE_1$	69.383	16.305	9.6	8.5	0.9	1.0	0.79	0.74
$ANDE_2$	69.391	15.598	23.2	16.9	0.7	1.0	0.87	0.63
$HARS_1$	69.232	16.535	48.2	4.0	1.1	1.1	0.78	0.78
$HARS_2$	69.642	16.683	94.1	25.6	0.8	0.8	0.82	0.75
$KABE_1$	67.723	13.435	70.4	24.5	1.5	0.9	0.63	0.67
$KABE_2$	67.686	14.185	60.5	8.9	1.3	1.1	0.74	0.76
$BODO_1$	67.511	14.380	25.4	3.8	1.8	1.4	0.74	0.70
$BODO_2$	67.685	14.173	45.7	9.4	1.3	1.1	0.72	0.76

[a]Chosen MSS observation sites contain Envisat and CTOH data. d_{TG} is the distance (in km) to the associated tide gauge, d_c is the distance (in km) to the coastline. $\hat{\sigma}$ is the estimated accuracy computed from the along-track altimetry data (in cm), and r_{TG} is the correlation of the altimetry data time series with the associated tide-gauge time series.

Table 5. MSS Observations From Altimetry South of 66°N (1996–2000)[a]

Site	φ (°)	λ (°)	d_{TG}	d_c	$\hat{\sigma}^{envi}$	$\hat{\sigma}^{ctoh}$	$\hat{\sigma}^{jas2}$	$\hat{\sigma}^{oce3}$	$\hat{\sigma}^{red3}$	r_{TG}^{envi}	r_{TG}^{ctoh}	r_{TG}^{jas2}	r_{TG}^{oce3}	r_{TG}^{red3}
$RORV_1$	65.029	10.579	36.2	4.7	0.9	0.8	0.6	0.6	0.6	0.85	0.67	0.67	0.57	0.46
$RORV_2$	65.639	10.474	93.9	36.4	0.7	0.8	0.5	0.5	0.5	0.62	0.49	0.56	0.37	0.19
$MAUS_1$	64.031	8.249	27.2	20.7	1.2	0.9	0.5	0.6	0.6	0.56	0.50	0.34	0.22	0.16
$MAUS_2$	64.138	7.775	52.9	44.1	1.1	1.0	0.4	0.5	0.5	0.50	0.53	0.37	0.25	0.12
$HEIM_1$	64.017	8.620	70.2	9.9	0.9	0.8	0.5	0.6	0.6	0.79	0.80	0.80	0.71	0.64
$HEIM_2$	63.778	7.382	93.9	38.7	0.9	0.9	0.4	0.5	0.5	0.55	0.54	0.62	0.35	0.20
$KRIN_1$	63.625	7.522	58.0	20.5	1.1	1.0	0.5	0.6	0.5	0.56	0.64	0.59	0.47	0.33
$KRIN_2$	63.652	6.768	77.0	52.8	0.9	0.8	0.4	0.5	0.4	0.61	0.56	0.56	0.28	0.07
$ALES_1$	62.846	6.015	42.6	12.4	1.1	1.1	0.6	0.6	0.6	0.73	0.81	0.64	0.55	0.49
$ALES_2$	63.312	6.150	94.0	50.5	0.8	0.8	0.4	0.4	0.4	0.68	0.54	0.54	0.30	0.30
$MALO_1$	62.266	4.591	45.9	27.5	0.8	0.8	0.5	0.6	0.6	0.65	0.64	0.66	0.45	0.43
$MALO_2$	62.266	3.868	74.8	63.5	0.7	0.8	0.4	0.5	0.5	0.58	0.67	0.52	0.24	0.24
$BERG_1$	60.470	4.669	36.7	8.9	0.9	0.9	0.5	0.6	0.6	0.66	0.61	0.60	0.45	0.45
$BERG_2$	60.667	4.095	73.6	33.0	0.5	0.8	0.5	0.6	0.6	0.44	0.25	0.42	0.34	0.24
$STAV_1$	59.384	4.640	77.2	14.8	0.8	0.9	0.6	0.6	0.6	0.43	0.41	0.51	0.46	0.39
$STAV_2$	59.734	4.753	101.4	18.2	1.4	0.9	0.6	0.6	0.6	0.55	0.38	0.54	0.46	0.43
$TREG_1$	57.898	7.992	28.5	16.3	1.3	1.2	0.7	0.7	0.8	0.48	0.52	0.50	0.45	0.48
$TREG_2$	57.271	7.762	83.0	49.9	1.0	1.0	0.7	0.7	0.7	0.53	0.47	0.45	0.39	0.38
$HELG_1$	58.394	9.734	67.4	43.2	1.0	0.9	0.6	0.7	0.6	0.37	0.33	0.34	0.33	0.23
$HELG_2$	58.340	9.978	73.4	58.0	1.4	1.1	0.5	0.6	0.5	0.30	0.32	0.33	0.24	0.18
$VIKE_1$	58.602	10.534	54.1	29.4	1.0	1.1	0.6	0.7	0.7	0.53	0.47	0.41	0.33	0.28

[a]Chosen MSS observation sites contain Envisat/CTOH and Jason-2/PISTACH data. d_{TG} is the distance (in km) to the associated tide gauge, d_c is the distance (in km) to the coastline. $\hat{\sigma}$ is the estimated accuracy computed from the along-track altimetry data (in cm), and r_{TG} is the correlation of the altimetry data time series with the associated tide-gauge time series.

$$z(t) = \alpha + \beta \cdot t + A_1 \sin(2\pi t - \varphi_1) + A_2 \sin(2\pi t/18.6 - \varphi_2), \quad (3)$$

where $z(t)$ is tide-gauge observation at epoch t, α is the intersect of the model, A_1, φ_1 are the amplitude and phase of the annual periodic variation, and A_2, φ_2 are the amplitude and phase of the nodal periodic variation [*Baart et al.*, 2012]. At most stations, the rate was estimated from a record covering the 1983–2013 period, but due to significant data gaps and short time series, the rates at Andenes and Mausund were estimated for the 1992–2013 period. As tide gauges provide relative observations of sea level, estimated rates need to be corrected for vertical land motion before they can be used to correct geocentric sea surface heights observed by altimetry. This was done by estimating vertical land motion from time series recorded at nearby permanent GNSS stations [*Kierulf et al.*, 2013].

With sea surface heights referenced to the mean epoch, cycle averages ($\overline{SSH}_{1998.5}$) were formed, and the mean sea surface was estimated by fitting equation (4) to the series of cycle averages (35 days for Envisat and 10 days for Jason-2):

$$\overline{SSH}_{1998.5}(t) = MSS_{1998.5} + A_1 \sin(2\pi t - \varphi_1), \quad (4)$$

where the annual term was included in order to reduce the variance of the adjustment and by that improve the possibility of detecting outliers. We note that ellipsoidal heights of MSS from Envisat refer to the WGS84 ellipsoid, likewise the Envisat-originated CTOH data. Jason-2/PISTACH, on the other hand gives MSS values above the TOPEX ellipsoid (with a semimajor axis of 6,378,136.3 m, and an inverse flattening of 1/298.25765). The ellipsoidal heights referenced to the TOPEX ellipsoid were transformed to WGS84 by first transforming the heights to Cartesian coordinates and then back to ellipsoidal heights above the WGS84 ellipsoid. The transformations were realized by standard formulas [e.g., *Hofmann-Wellenhof et al.*, 2001, chapter 10].

Finally, in addition to the five monomission along-track data sets, we have considered the Technical University of Denmark (DTU) multimission MSS model DTU13MSS [*Andersen et al.*, 2013], available at ftp://ftp.space.dtu.dk/pub/DTU13/. It is given on a global $1' \times 1'$ grid and is a development of the former DNSC08 MSS model [*Andersen and Knudsen*, 2009], with standard range corrections applied (Table 3). DTU13MSS is averaged over the period 1993–2012 and offers an increased amount of retracked coastal satellite altimetry data, data from the Jason-1 geodetic mission, as well as a combination of ERS-1/ERS-2/Envisat and Cryosat-2 altimetry data in the northern high latitudes. DTU13MSS is also referred to the TOPEX ellipsoid and was referenced to WGS84 by computing an average difference of 0.686 m between regional geoids synthesized

with WGS84 and TOPEX ellipsoidal parameters, and subtracting this difference from the MSS values. DTU13MSS was adjusted to the 1996–2000 period using equation (2).

2.1.4. Geodetic MDT

Determining the geodetic MDT is closely related to the method of combining GNSS and leveling on land, cf. equation (1):

$$\mathrm{MDT} = h - \zeta, \tag{5}$$

where h is the ellipsoidal height of MSS or MSL at altimetry or tide-gauge sites, respectively, and ζ is the height anomaly, all referring to the same reference ellipsoid.

Height anomalies from the four quasigeoid model grids (Table 6) were linearly interpolated to the altimetry and tide-gauge sites (Tables 2, 4, and 5) by nearest neighbor, before subtraction by equation (5).

2.2. Ocean Approach

The geodetic MDT estimates were validated using numerical ocean models independent of geodetic data (as opposed to assimilated models incorporating geodetic data). Such models employ forcings in the form of in situ hydrographic data sets (salinities and temperatures) and meteorological information, where the MDT reflects the mean dynamical response of the ocean model to these forcings, determined by the equations of motion. In this work, six numerical ocean models have been used (Table 6).

Five of the ocean models were provided by the National Oceanography Centre (C. W. Hughes, personal communication, 2014). In particular, there are two Nemo (Nucleus for European Modelling of the Ocean) ORCA [*Madec*, 2008] model integrations, one at a resolution of $1/4^\circ$ (NemoQ), and one at a resolution of $1/12^\circ$ (Nemo12). Then come two Liverpool University implementations of the Massachusetts Institute of Technology (MIT) global ocean circulation model [*Marshall et al*., 1997a, 1997b], assimilating hydrographic information provided by the UK Met Office [*Smith and Murphy*, 2007]; one in a coarse form (L-MITc), with a global resolution of 1°, and a finer version (L-MITf) with an increased resolution of $1/5^\circ \times 1/6^\circ$ in the North Atlantic. Finally, there is the Ocean Circulation and Climate Advanced Modeling (OCCAM) $1/12^\circ$ global ocean circulation model [*Marsh et al*., 2009]. The ocean models incorporate a climatology for their initiation, as well as wind and atmospheric forcing from meteorological reanalyses. All models are averaged over the period 1996–2000 inclusive, which set the standardization epoch for all data sets.

The five mentioned ocean models have their primary application in deep ocean studies, rather than in studies of the coastal zone, and their spatial resolutions are insufficient to resolve many coastal processes (e.g., river runoff) [*Woodworth et al*., 2012]. Therefore, we have also considered the Proudman Oceanographic Laboratory Coastal Modelling System (POLCOMS) coastal model [*Holt and James*, 2001], distributed by the British Oceanographic Data Centre at http://www.bodc.ac.uk. Yearly model runs were averaged over the 1996–2000 period. With a $1/9^\circ \times 1/6^\circ$ resolution, this model is used for studies of continental shelf processes, and takes river runoff into account. Regrettably, the model does not cover the entire Norwegian coast (see Table 6) but has been included in the analysis for tide-gauge and altimetry sites south of 65°N.

As part of earlier work, the global ocean models provided to us have been resampled to common $1/4^\circ \times 1/4^\circ$ grids by nearest-neighbor linear interpolation to facilitate intercomparison studies (C. W. Hughes, personal communication, 2015). In the present work, these grids were further linearly interpolated to the altimetry and tide-gauge sites (Tables 2, 4, and 5) by nearest neighbor.

We investigated how the intermediate $1/4^\circ \times 1/4^\circ$ interpolation might affect the final MDT values by resampling POLCOMS in the same manner, and comparing values at the altimetry and tide-gauge sites with the ones directly interpolated from the native POLCOMS grid. The standard deviation of differences between native and resampled POLCOMS values was found to be ~1 cm. This impacts the final results (Tables 7 and 8) on the submillimeter level; thus, we do not expect a significant error due to the intermediate interpolation.

We further compared linearly interpolated with bicubically interpolated ocean MDTs, and observed an improvement (reaching 9 mm with Nemo12) with the bicubically interpolated values at the altimetry sites. Simultaneously, however, a degradation was observed (reaching 12 mm, again with Nemo12) with the bicubically interpolated values at the tide gauges. Due to this ambiguity, we decided to retain the linearly interpolated values for all altimetry and tide-gauge sites.

Table 6. Model Grids Used in Our Work

Model	Coverage	Time Period	Grid Spacing (°) or d/o	Reference
Quasigeoid[a]				
TIM5+NMA2014	$57^\circ \le \varphi \le 73.99^\circ$ $-11^\circ \le \lambda \le 36^\circ$		0.01×0.02	This work
DIR5+NMA2014	$57^\circ \le \varphi \le 73.99^\circ$ $-11^\circ \le \lambda \le 36^\circ$		0.01×0.02	This work
NMA2014	$53^\circ \le \varphi \le 77.99^\circ$ $-15^\circ \le \lambda \le 40^\circ$		0.01×0.02	NMA
EGM2008	Global		2190	*Pavlis et al.* [2012]
MSS[b]				
DTU13MSS	Global	1993–2012	1/60×1/60	*Andersen and Knudsen* [2009], *Andersen et al.* [2013]
Ocean[c]				
Nemo12	Global	1996–2000	1/12×1/12	*Blaker et al.* [2015] ,
NemoQ	Global	1996–2000	1/4×1/4	*Madec* [2008]
L-MITf[d]	Global	1996–2000	1/5×1/6	*Marshall et al.* [1997a],
L-MITc	Global	1996–2000	1×1	*Marshall et al.* [1997b], *Smith and Murphy* [2007]
OCC12	Global	1996–2000	1/12×1/12	*Marsh et al.* [2009], *Webb et al.* [1997]
POLCOMS	$40.0556^\circ \le \varphi \le 64.8889^\circ$ $-19.9167^\circ \le \lambda \le 13^\circ$	1996–2000	1/9×1/6	*Holt and James* [2001]

[a]All quasigeoid models were equally arranged on the grid delimited by $57^\circ \le \varphi \le 73.99^\circ$, $-11^\circ \le \lambda \le 36^\circ$, and with $0.01^\circ \times 0.02^\circ$ spacing. Next, the geoid values were linearly interpolated to the altimetry and tide-gauge sites (Tables 2, 4, and 5) by nearest neighbor.
[b]DTU13MSS was linearly interpolated to the altimetry sites (Tables 4 and 5).
[c]All ocean models were linearly interpolated to the altimetry and tide-gauge sites (Tables 2, 4, and 5) by nearest neighbor.
[d]This grid spacing covers the North Atlantic, and gradually spreads to $1^\circ \times 1^\circ$ elsewhere.

Any ocean model including air pressure forcing was corrected for it before being provided to us (Hughes, personal communication, 2015). POLCOMS also includes an IB correction as described in section 2.1.2, with a reference pressure of 1012 mbar (J. T. Holt, personal communication, 2015). We used a simple approach to revert the interpolated $MDT_{POLCOMS}$ values. At each tide-gauge site with associated altimetry sites, the IB correction was subtracted. For this we used the single pressure value that was used to correct tide-gauge MSL.

3. Comparative Assessment

We have focused our analysis on the entire Norwegian coast, because it yields the most robust statistics. However, due to the limited spatial coverage of the Jason-2/PISTACH and POLCOMS data sets (sections 2.1.3 and 2.2), we also present results from the regions south and north of 66°N.

3.1. Tide-Gauge MDT

Table 7 shows standard deviations of differences between tide-gauge geodetic and ocean MDTs, using ellipsoidal heights of MSL determined from NN2000 and NN1954 data. We first note that geodetic and ocean MDTs agree on the ∼3–7 cm level. This is an encouraging observation, as similar studies for tide gauges along other coasts have shown an agreement between geodetic and ocean MDTs on the ∼6–14 cm level [e.g., *Woodworth et al.*, 2012, 2015]. *Higginson et al.* [2015] got an agreement between geodetic and ocean MDTs of 2.3 cm along the east coast of North America; however, this number resulted from mean geodetic and ocean MDTs based on 7 geoid models and 11 ocean models, respectively.

On average, NN2000-based geodetic MDTs score better than NN1954-based geodetic MDTs for all ocean models. The lowest standard deviations are found when geodetic MDTs are compared with MDT_{Nemo12}, and the highest when compared with $MDT_{L\text{-}MITc}$. The GOCE R5 models outperform NMA2014.

The along-shore tide-gauge geodetic and ocean MDT profiles are shown in Figure 2. All MDTs show similar general traits; MDT rises 10 cm from Vardø to Kabelvåg, then flattens out to Stavanger, and rises another 10 cm toward Viker. The geodetic profiles present a greater variation in MDT than the ocean models. The ocean profiles (Figure 2a) have an average standard deviation of 5.7 cm, while the average standard deviations of the NN1954-based and NN2000-based geodetic profiles (Figures 2b and 2c) are 7.0 and 5.9 cm, respectively. MDT_{Nemo12} is plotted together with the geodetic MDTs to allow for easier comparison, as it is

Table 7. Standard Deviations of Differences Between Tide-Gauge Geodetic and Ocean MDTs (cm)

	Nemo12	NemoQ	L-MITf	L-MITc	OCC12	POLCOMS[a]
Entire Coast						
NN2000 DIR5+NMA2014	3.8	4.1	4.2	4.9	4.9	
NN2000 TIM5+NMA2014	3.8	4.2	4.3	5.0	5.0	
NN2000 NMA2014	4.4	4.8	4.6	5.5	5.6	
NN2000 EGM2008	3.7	3.5	5.0	4.9	4.5	
NN1954 DIR5+NMA2014	4.2	4.5	5.2	5.4	5.2	
NN1954 TIM5+NMA2014	4.3	4.5	5.3	5.5	5.3	
NN1954 NMA2014	4.6	5.0	5.3	5.8	5.7	
NN1954 EGM2008	5.1	5.0	6.6	6.2	5.7	
North of 66°N						
NN2000 DIR5+NMA2014	5.1	5.1	4.0	5.4	5.9	
NN2000 TIM5+NMA2014	5.1	5.2	4.1	5.6	6.0	
NN2000 NMA2014	5.8	5.9	4.8	6.3	6.7	
NN2000 EGM2008	4.5	4.3	4.3	5.4	5.8	
NN1954 DIR5+NMA2014	4.7	5.0	4.3	4.7	5.5	
NN1954 TIM5+NMA2014	4.8	5.0	4.4	4.8	5.6	
NN1954 NMA2014	5.2	5.4	4.7	5.3	6.1	
NN1954 EGM2008	5.9	5.9	6.2	6.3	6.8	
South of 66°N						
NN2000 DIR5+NMA2014	2.8	2.7	3.7	4.6	3.8	4.2
NN2000 TIM5+NMA2014	2.8	2.7	3.7	4.7	3.9	4.2
NN2000 NMA2014	3.1	3.1	4.1	4.9	4.1	4.5
NN2000 EGM2008	3.1	2.9	3.5	4.7	3.4	4.8
NN1954 DIR5+NMA2014	4.0	4.2	4.8	6.2	5.2	5.1
NN1954 TIM5+NMA2014	4.0	4.3	4.9	6.2	5.2	5.1
NN1954 NMA2014	4.3	4.5	5.1	6.4	5.4	5.4
NN1954 EGM2008	4.3	4.4	4.7	6.3	5.0	5.7

[a]For POLCOMS, the analysis covers the Norwegian coast south of 65°N.

the best-performing ocean model. As concluded from Table 7, the general agreement between geodetic and ocean MDTs increases when using NN2000-based geodetic estimates. We further note that $MDT_{POLCOMS}$ performs on the same level as the remaining ocean MDTs, although it does not observe the 10 cm rise from Stavanger toward Viker.

3.2. Altimetric MDT

Table 8 shows standard deviations between altimetric geodetic and ocean MDTs. Geodetic and ocean MDTs agree on the ~5–11 cm level. To our knowledge, no comparisons of geodetic MDTs based on pointwise altimetry with pure ocean MDTs have been made. However, *Thompson et al.* [2009] compared zonal and meridional sections of ocean and geodetic (computed by subtracting a GRACE-based regional geoid model from an altimetric MSS product) MDT grids in the North Atlantic Ocean, and obtained an agreement

Table 8. Standard Deviations of Differences Between Altimetric Geodetic and Ocean MDTs (cm)

	Nemo12	NemoQ	L-MITf	L-MITc	OCC12		Nemo12	NemoQ	L-MITf	L-MITc	OCC12	POLCOMS[a]
Entire Coast						**South of 66°N**						
envi DIR5+NMA2014	6.4	7.1	8.2	8.7	7.3	envi DIR5+NMA2014	5.2	7.0	7.6	9.6	7.7	5.3
envi TIM5+NMA2014	6.3	7.1	8.2	8.8	7.3	envi TIM5+NMA2014	5.0	7.0	7.6	9.5	7.6	5.1
envi NMA2014	6.6	7.2	8.3	8.7	7.3	envi NMA2014	5.0	6.8	7.2	9.2	7.2	4.8
envi EGM2008	5.7	6.7	6.3	8.1	7.1	envi EGM2008	5.7	6.2	6.0	7.4	7.2	5.5
ctoh DIR5+NMA2014	7.4	8.1	9.3	9.9	8.6	ctoh DIR5+NMA2014	5.9	7.9	8.7	10.5	9.0	6.2
ctoh TIM5+NMA2014	7.4	8.1	9.3	9.9	8.6	ctoh TIM5+NMA2014	5.8	7.9	8.7	10.5	9.0	6.0
ctoh NMA2014	7.6	8.3	9.3	9.9	8.7	ctoh NMA2014	5.6	7.6	8.3	10.1	8.6	5.7
ctoh EGM2008	6.4	7.4	7.2	9.0	8.1	ctoh EGM2008	5.7	6.7	6.9	8.1	8.1	5.6
dtu13 DIR5+NMA2014	5.6	6.5	7.5	8.4	6.7	dtu13 DIR5+NMA2014	5.3	6.6	7.4	9.1	7.1	5.0
dtu13 TIM5+NMA2014	5.5	6.5	7.5	8.5	6.8	dtu13 TIM5+NMA2014	5.2	6.6	7.5	9.1	7.1	4.9
dtu13 NMA2014	5.7	6.5	7.5	8.4	6.7	dtu13 NMA2014	5.2	6.4	7.1	8.7	6.7	4.6
dtu13 EGM2008	6.1	7.1	6.4	8.6	7.6	dtu13 EGM2008	5.4	5.4	5.4	6.5	6.2	4.7
North of 66°N						jas2 DIR5+NMA2014	5.4	6.7	7.6	9.4	7.8	5.4
envi DIR5+NMA2014	7.2	7.3	7.5	7.8	7.0	jas2 TIM5+NMA2014	5.2	6.6	7.5	9.3	7.8	5.2
envi TIM5+NMA2014	7.3	7.3	7.5	7.9	7.0	jas2 NMA2014	5.2	6.4	7.2	9.0	7.4	4.9
envi NMA2014	7.8	7.8	7.9	8.4	7.6	jas2 EGM2008	6.5	6.4	6.6	7.6	7.8	6.1
envi EGM2008	5.2	5.8	6.8	6.1	5.0							
						oce3 DIR5+NMA2014	5.5	6.2	7.0	8.7	7.4	6.1
ctoh DIR5+NMA2014	8.8	8.6	8.7	9.3	8.4	oce3 TIM5+NMA2014	5.4	6.1	7.0	8.7	7.3	5.9
ctoh TIM5+NMA2014	8.8	8.7	8.8	9.4	8.5	oce3 NMA2014	5.3	5.9	6.6	8.3	7.0	5.7
ctoh NMA2014	9.4	9.2	9.3	10.0	9.1	oce3 EGM2008	6.4	5.7	5.7	6.7	7.2	6.7
ctoh EGM2008	6.7	7.0	7.8	7.6	6.4							
						red3 DIR5+NMA2014	5.3	5.4	6.3	8.1	6.6	6.3
dtu13 DIR5+NMA2014	6.0	6.4	7.1	7.3	6.3	red3 TIM5+NMA2014	5.1	5.3	6.3	8.0	6.5	6.1
dtu13 TIM5+NMA2014	6.1	6.4	7.1	7.3	6.4	red3 NMA2014	5.1	5.1	5.9	7.6	6.1	5.9
dtu13 NMA2014	6.5	6.8	7.3	7.8	6.9	red3 EGM2008	6.6	5.3	5.3	6.2	6.7	7.3
dtu13 EGM2008	4.8	5.8	7.2	6.5	5.3							

[a]For POLCOMS, the analysis covers the Norwegian coast south of 65°N.

of 8 cm between the grids. *Woodworth et al.* [2015] obtained an agreement of 6 cm between a geodetic MDT grid (computed by subtracting a DIR5-based geoid from an altimetric MSS product) and an assimilated MDT grid in the Mediterranean. They further conclude that ∼5 cm is a likely general level of agreement between altimetric geodetic and ocean MDT grids. This work shows that pointwise monomission coastal altimetry products give results comparable with the multimission DTU13MSS grid on the ∼5 cm level, which is encouraging.

As with the tide gauges, on average, we observe lowest standard deviations when comparing geodetic MDTs with MDT_{Nemo12}, and highest when comparing with $MDT_{L\text{-}MITc}$. As with the tide-gauge geodetic MDTs, we note that the GOCE R5 models outperform NMA2014. We further observe that $MDT_{POLCOMS}$ performs well, on the level of MDT_{Nemo12}. The poorest altimetry performance is delivered by CTOH, regardless of quasigeoid model.

Figure 3 shows the along-shore altimetric geodetic and ocean MDT profiles for the entire coast. Even though the pattern complexity has increased, it is still possible to infer the MDT rise from Vardø to Kabelvåg, as well as a flattening toward Heimsjø. A distinctive fall of MDT is observed by all MDT models toward Bergen 2. Another fall is observed by MDT_{Nemo12} and the geodetic MDTs from Tregde toward Helgeroa, which is not observed by the remaining ocean models.

In the cases where the distances between two associated MSS sites and the coast differ considerably (e.g., Rørvik 1 and Rørvik 2), so will their MDT value, because the MDT is higher toward the coast. This explains the zigzag pattern we observe when following the profile lines with their alternating order of sites closer to, respectively further off the coast (Figure 3a).

The ocean profiles (Figure 3a) present an average standard deviation of 4.9 cm, while the geodetic profiles (Figures 3b–3d) based on Envisat, CTOH, and DTU13MSS present larger values of 7.0, 8.1, and 6.5 cm, respectively.

The along-shore altimetric geodetic and ocean MDT profiles south of 66°N are shown in Figure 4, beginning at Rørvik 2. In Figure 4a, we see that the course of $MDT_{POLCOMS}$ observes the same fall from Tregde toward Helgeroa as MDT_{Nemo12} and the geodetic MDTs. The course of the Jason-2-based MDT profiles (Figures 4b–4d) generally agrees well with the Envisat-based MDT profiles south of 66°N.

3.3. Comparison of Taylor Diagrams

A Taylor diagram [*Taylor*, 2001] summarizes four model statistics in a single diagram. If we consider two models, the four statistics are the model standard deviations (σ_1, σ_2), their correlation R, and the centered

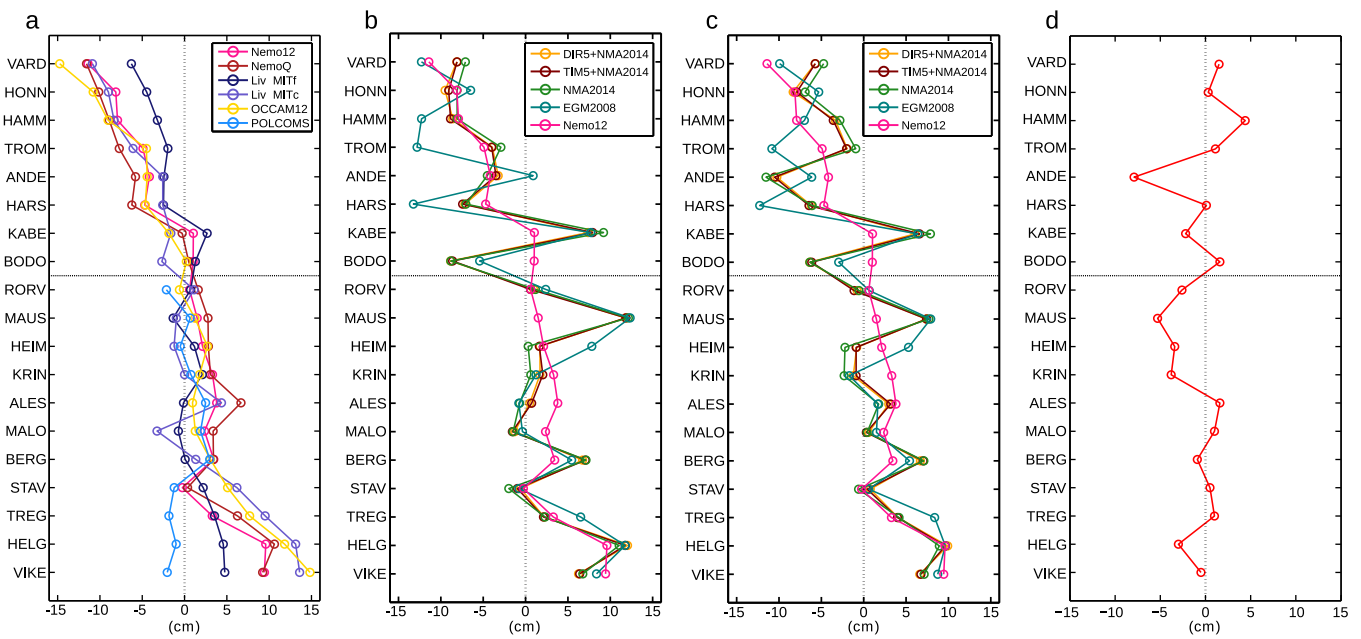

Figure 2. Tide-gauge MDT profiles: (a) ocean, (b) geodetic, using NN1954-originated ellipsoidal heights of MSL, (c) geodetic, using NN2000-originated ellipsoidal heights of MSL, and (d) the difference between NN1954-originated and NN2000-originated MDT. In Figures 2b and 2c, MDT_{Nemo12} is included. The horizontal dashed line denotes 66°N. In all cases, the profile mean has been removed.

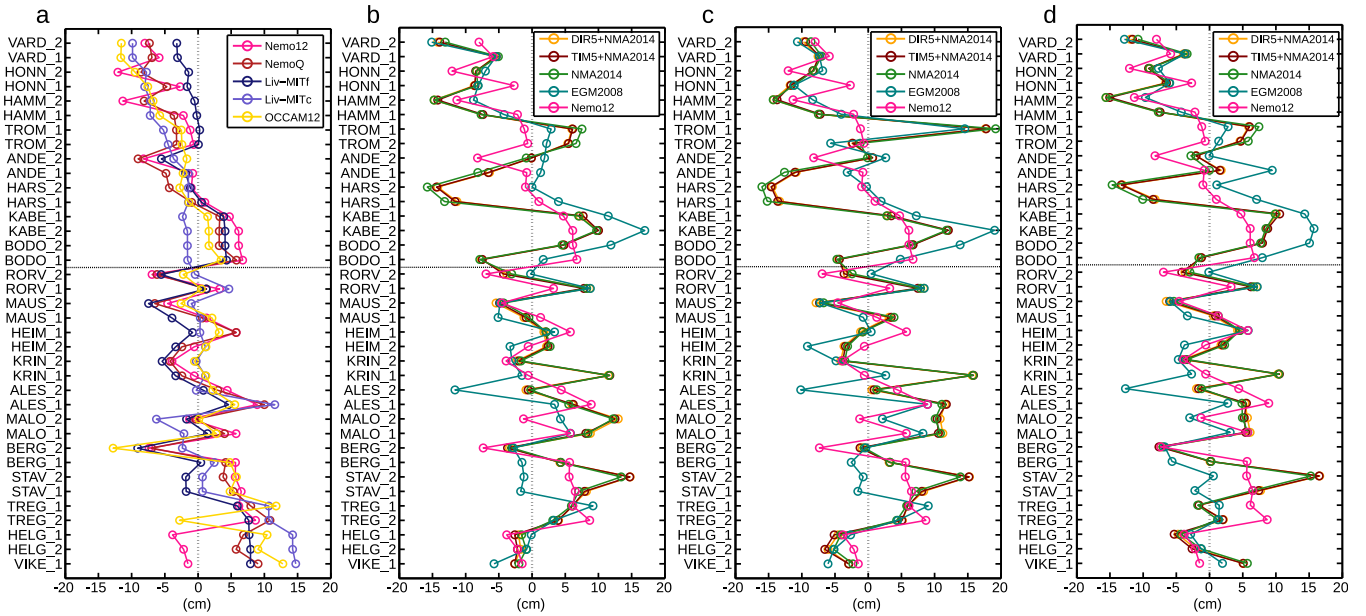

Figure 3. Altimetric MDT profiles along the entire Norwegian coast: (a) ocean, (b) geodetic, using Envisat, (c) geodetic, using CTOH, and (d) geodetic, using DTU13MSS. In Figures 3b–3d, MDT_{Nemo12} is included. The horizontal dashed line denotes 66°N. In all cases, the profile mean has been removed.

root-mean-square (RMS) difference between the models E', related by $E'^2=\sigma_1^2+\sigma_2^2-2\sigma_1\sigma_2 R$. This relation has an analogue in the cosine rule for triangles, which is exploited in the Taylor diagram. It allows for convenient model intercomparison and was applied to MDTs by *Bingham and Haines* [2006].

Figure 5 shows Taylor diagrams where MDT_{Nemo12} has been chosen as the reference model against which all other MDTs are compared. It was chosen because, on average, it is the best-performing ocean model. The model standard deviations are represented as radial distances from the origin, the centered RMS differences are proportional to the distances between reference and test models, and correlations are represented as the azimuthal angle. Consequently, the reference model has a correlation of one.

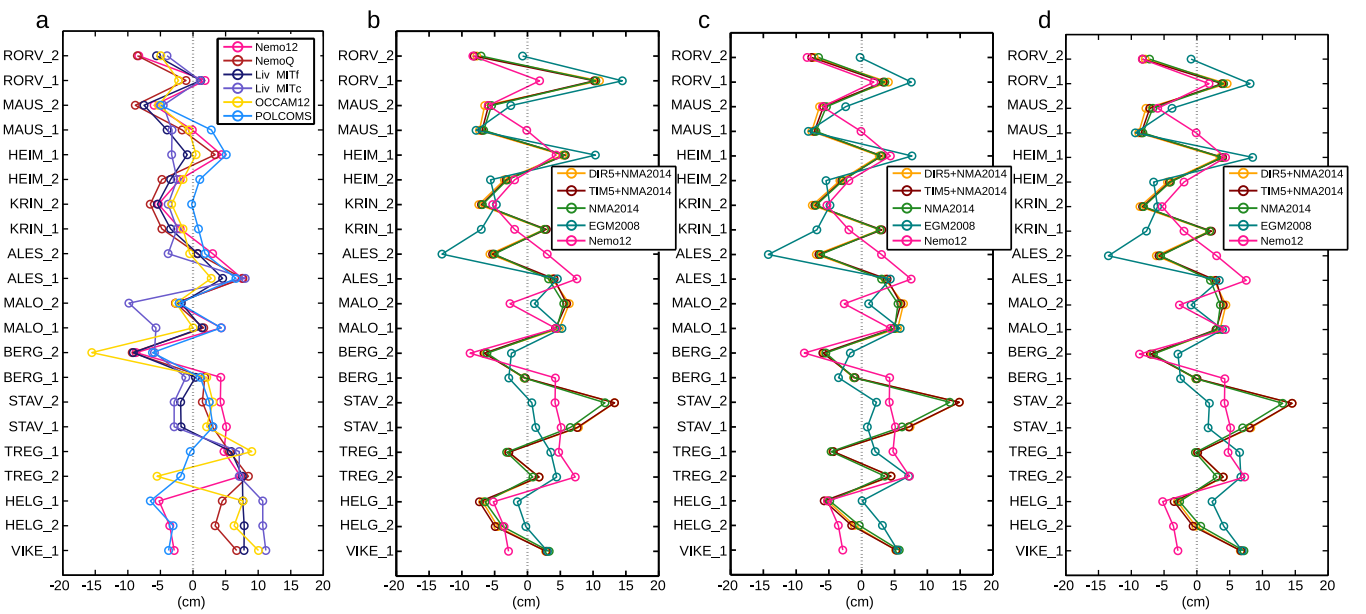

Figure 4. Altimetric MDT profiles along the Norwegian coast south of 66°N: (a) ocean, (b) geodetic, using Jason-2, (c) geodetic, using Ocean3, and (d) geodetic, using Red3. In Figures 4b–4d, MDT_{Nemo12} is included. In all cases, the profile mean has been removed.

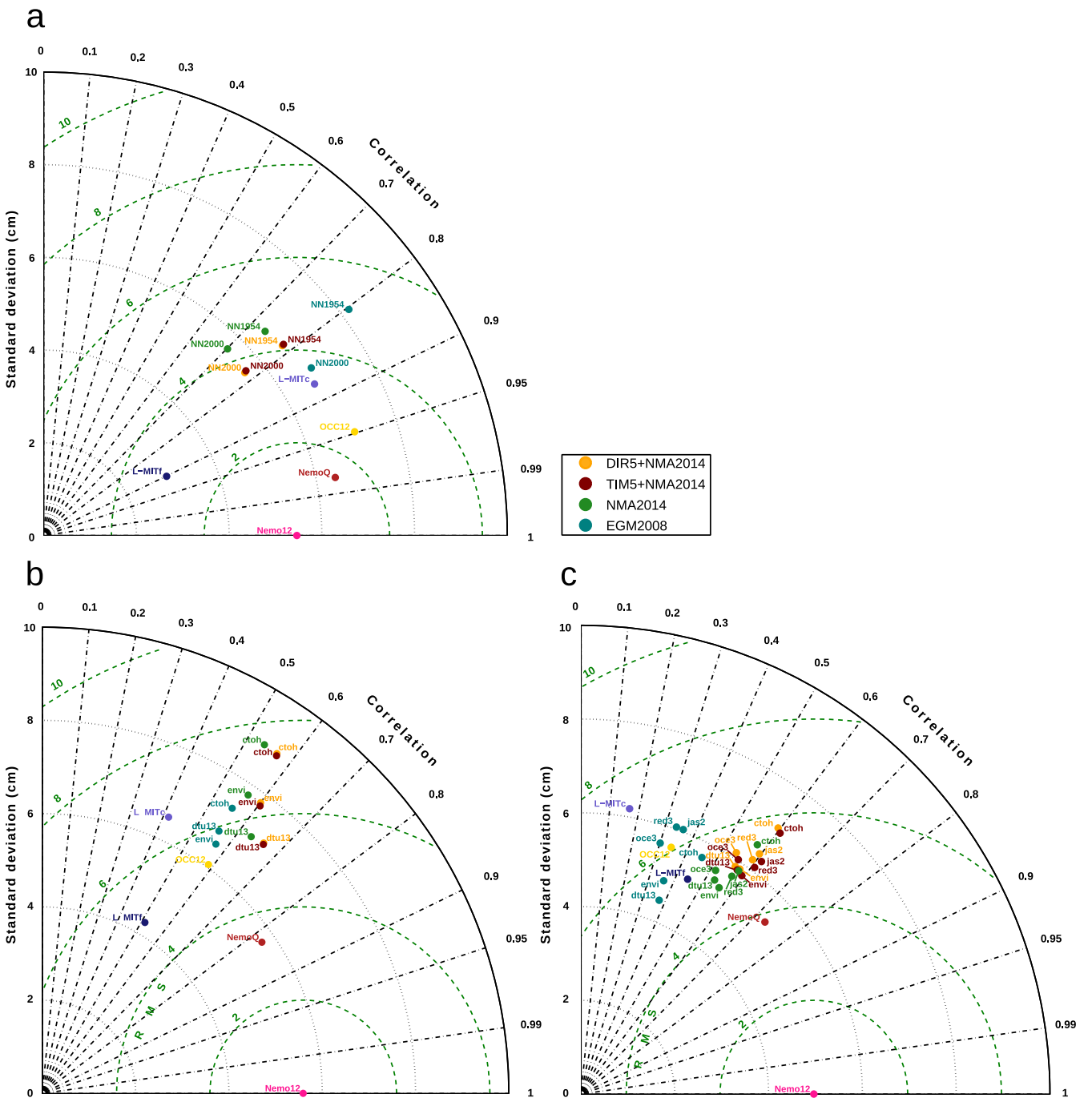

Figure 5. Taylor diagram intercomparison of geodetic and ocean MDTs for tide gauges (a) along the entire Norwegian coast, altimetric MSS sites (b) along the entire Norwegian coast, and (c) south of 66°N. To ease readability, labels for the geoid models incorporated in the geodetic MDTs have been left out of the diagrams; however, this information may be inferred from the legend.

Figure 5a shows the Taylor diagram for tide-gauge geodetic and ocean MDTs along the entire coast. As MDT_{NemoQ} is closely related to the reference model, it consequently has the lowest RMS difference and highest correlation. Geodetic MDTs based on EGM2008 have a higher correlation than the NMA2014-related MDTs, but generally the geodetic MDTs give quite similar results. Almost all MDTs but the NN1954-based geodetic MDTs lie within an RMS of 4 cm.

Figures 5b and 5c show results from the altimetric geodetic and ocean MDTs along the entire coast as well as south of 66°N. We observe that the ocean MDTs are more similar to MDT_{Nemo12} considering the entire

coast than south of 66°N. Furthermore, the signal standard deviations of the geodetic MDTs are lower south of 66°N than for the entire coast, suggesting that the geodetic MDTs are a little smoother in the south. This explains why the MDT values in Table 8 vary primarily by geodetic MDT north of 66°N, while varying primarily by ocean MDT south of 66°N.

4. Discussion

4.1. Error Budgeting and Significance of Results

Using the standard deviations of differences between geodetic and ocean MDTs (Tables 7 and 8) we derive error estimates for both. We relate the empirical standard deviation of differences, $s=\sqrt{\sum_{i=1}^{n}(\epsilon_i-\bar{\epsilon})^2/(n-1)}$, where $\epsilon=\mathrm{MDT}-(h-\zeta)$, to the formal error propagation $\sigma=\sqrt{\sigma_{\mathrm{MDT}}^2+\sigma_h^2+\sigma_\zeta^2}$. Here we take MDT to be the ocean model, h to be the ellipsoidal height of tide-gauge MSL or altimetric MSS, and ζ to be the height anomaly. Consequently, σ_{MDT}, σ_h, and σ_ζ are the error contributions from ocean model, ellipsoidal height, and quasigeoid model, respectively. By this approach, we assume that the individual components are uncorrelated, because they are derived from independent methods.

We turn to Table 1, and, assuming equal error contribution from quasigeoid, leveling and GNSS, derive an estimate $\sigma_\zeta \approx 2$ cm. This estimate is based on the NMA2014-related quasigeoids. We did not consider EGM2008 because we trace its worse performance to the slightly lower resolution compared to the NMA2014-related quasigeoids. Furthermore, we take $\sigma_h \approx 1$ cm, corresponding to the lower HREF error estimate of *Mysen* [2014]. Using these numbers together with the standard deviations s from Table 7 (entire coast, and NN2000), we get $\sigma_{\mathrm{MDT}} \approx 3-5$ cm, depending on the ocean model. Because σ_ζ is derived from an assumption of equal error contribution from quasigeoid, leveling, and GNSS, rather than from error propagation of the heterogeneous gravity data included in the quasigeoid model, we take it to be an optimistic estimate. Furthermore, the HREF error estimate σ_h is inherently optimistic due to different aspects of the estimation method of *Mysen* [2014]. Consequently, as we regard our estimates of σ_ζ and σ_h as optimistic, σ_{MDT} is a pessimistic estimate. Alternatively, assuming equal error contributions from σ_ζ, σ_h, and σ_{MDT}, we get $\sigma_{\mathrm{MDT}} \approx 2-3$ cm.

It is more challenging to assess the quasigeoid error off the coast. Therefore, we choose the more conservative estimate of $\sigma_\zeta \approx 3$ cm. We do not expect the ocean models to be more accurate at the tide gauges than at the altimetry sites (in fact, the opposite is more likely). Consequently we adopt $\sigma_{\mathrm{MDT}} \approx 2-5$ cm. Using these numbers together with the standard deviations s from Table 8 (entire coast, Nemo12), we get $\sigma_h \approx 1-7$ cm for the altimetric MSS. We have chosen Nemo12 because it shows the lowest s values, and larger values are attributed to σ_{MDT} and not σ_h. Alternatively, if we assume equal error contributions from σ_ζ, σ_h, and σ_{MDT}, we get $\sigma_{\mathrm{MDT}} \approx 3-4$ cm.

When summarizing the error estimates at the tide-gauge and altimetry sites, we conclude that $\sigma_\zeta \leq 4$ cm, $\sigma_{\mathrm{MDT}} \leq 5$ cm, and $\sigma_h \leq 7$ cm.

We further want to comment on the significance of our results. Looking at the Taylor diagram at the altimetry sites (Figure 5b), we see that the signal standard deviation of the geodetic MDTs is roughly 7 cm. From our altimetry error estimates, we derive an error standard deviation for the geodetic MDTs of 2–8 cm, which gives a signal-to-noise ratio (SNR) of 1–3. This suggests that our results at the altimetry sites are statistically significant. From Figure 5b, we also find a ~60% correlation of the geodetic MDTs with $\mathrm{MDT}_{\mathrm{Nemo12}}$. This value proves actual correlation with a certainty of 99%, as confirmed by a correlation significance test. At the tide gauges (Figure 5a), the signal standard deviation of the geodetic MDTs is roughly 6 cm. The tide-gauge error estimates give an error standard deviation of 2–4 cm for the geodetic MDTs, again resulting in an SNR of 1–3. Furthermore, we observe an even higher ~80% correlation of the geodetic MDTs with $\mathrm{MDT}_{\mathrm{Nemo12}}$ than at the altimetry sites. Thus, we consider our results statistically significant.

4.2. Tide-Gauge MDT

Considering the assessment of geodetic MDTs at Norwegian tide gauges, standard deviations of differences suggest an improvement when using data based on the new height system, NN2000. North of 66°N, improvement is less evident. We note a possible explanation for the worse fit of tide-gauge geodetic MDTs

north of 66°N. As mentioned, Norway is in the process of changing its height system from NN1954 to NN2000, and at the time of writing, no municipalities north of 66°N have initiated the change. Consequently, HREF2014c should not be considered a final HRCS for NN2000, and changes are expected in future versions (D. I. Lysaker, NMA, personal communication, 2015). As the largest discrepancies between NN1954 and NN2000 are found in Northern Norway, this might be part of the explanation. We thus expect that with the finalization of the height system change, better results will be obtained when using data based on the new height system, NN2000. Better still, using GNSS to directly observe ellipsoidal height of MSL at the tide gauges would eliminate this uncertainty altogether.

4.3. Altimetric MDT

Regarding the altimetry-based geodetic MDTs, we note that those based on DTU13MSS perform well in all regions. One of the reasons for the good performance of DTU13MSS could be that it contains an increased amount of altimetry observations from several altimeters, including the more recent Cryosat-2 mission. Another reason could be that it is a gridded product. Gridding will to some extent always imply an unwanted smoothing, as values at equally spaced grid points are estimated from irregularly distributed data through spatiotemporal interpolation. Thus, DTU13MSS may well be more similar to the ocean models, which are also smooth surfaces not only due to their initial model physics and grids but also due to resampling (section 2.2).

We should also mention that *Woodworth et al*. [2015] considered DTU10MSS rather than DTU13MSS in the Mediterranean, as the latter model showed more spatial differences than was expected from the few additional years of observations. Our analysis with DTU10MSS along the Norwegian coast, however, gave slightly worse results than with DTU13MSS, which suggests that DTU13MSS offers an improvement over DTU10MSS along the Norwegian coast.

In general, CTOH performance is poor, which is not easily explained. Part of the explanation may be that CTOH uses the radiometer for the wet tropospheric correction, while Envisat and Jason-2/PISTACH use a composite model, exchanging the radiometer for ECMWF data within 50 km of the coast. However, DTU13MSS also uses the radiometer for the wet tropospheric correction, which suggests that differences in the correction method (radiometer or ECMWF) are of minor importance.

The performance of Jason-2/PISTACH corresponds well with Envisat for all ocean models. On average, Ocean3 offers a slight improvement over Jason-2, and Red3 an improvement over Ocean3 (Red3 differs from Jason-2 and Ocean3 in that it uses GIM only for the ionospheric correction, and lacks correction for the sea-state bias). However, we conclude that improvements due to retracking are small compared with the differences observed between different quasigeoid models.

From the Taylor diagram intercomparison at the altimetry sites, we observe that geodetic MDTs based on both pointwise and gridded altimetry correlate more with MDT_{Nemo12} than do $MDT_{L\text{-}MITc}$, $MDT_{L\text{-}MITf}$, and MDT_{OCC12}, suggesting a convergence of the geodetic and ocean MDT approaches.

4.4. Characteristics of Coastal MDT in Norway

The tide-gauge and altimetric geodetic MDT profiles generally show a similar pattern (a 10 cm rise toward Kabelvåg, a flattening toward Stavanger, and another 10 cm rise toward Viker), although with some differences. In part, these differences result from the geographic location of the tide-gauge and altimetry sites (Figure 1).

At the tide gauges, the rise from Stavanger southward is evident in all ocean MDTs but $MDT_{POLCOMS}$ (Figure 2). This rise is confirmed by the geodetic MDTs regardless of quasigeoid model or height system, which suggests that the MDT along the southern coast is not well represented in $MDT_{POLCOMS}$. The general tendency of lower MDT values at the altimetry sites further off the coast is evident in all geodetic MDTs and MDT_{Nemo12}, but not in the remaining ocean MDTs (Figure 3). This suggests that the MDT characteristics along the southern coast of Norway are best described by MDT_{Nemo12} as opposed to the other ocean models.

If a tide gauge is located in a protected harbor, or in the vicinity of an estuary, observed MSL may include a steric contribution from river runoff and other coastal processes that the altimetry observations lack. All geodetic MDTs observe large variations in the Lofoten Basin (covered by Kabelvåg and Bodø) that are not

observed by the ocean MDTs. This, however, is an area of considerable dynamic activity in the form of maelstroms and eddies, and the ocean models are likely to have limited validity in this area.

In general, we observe more variability in the geodetic MDTs than in the ocean MDTs. This may be attributed to observation errors in the geodetic MDTs, but also to the smooth characteristics of the ocean models, which have their main application in the open ocean, resolving features at larger spatial scales. Generally, the spatial scale of MDT will depend on the temporal averaging period, as well as the length scale at which geostrophic currents (determined from the MDT inclination) become important. This length scale, known as the Rossby radius of deformation, depends on the Coriolis parameter, and thus varies with latitude (∼200 km close to the equator, ∼10 km at high latitudes). In addition, at the coast, ocean dynamic features not yet fully understood, exist at shorter scales than on the open ocean. Therefore, it is likely that part of the variability observed by geodetic observations comes from actual short-scale ocean dynamics not resolved by the general circulation models.

Consequently, we would expect $MDT_{POLCOMS}$, which takes shorter-scale coastal shelf processes into account, to show a better agreement with the geodetic MDTs than the other ocean MDTs. While scoring well at the altimetry sites, in close agreement with MDT_{Nemo12}, and corresponding well to the geodetic MDTs, it lags behind at the tide gauges.

It generally remains challenging to assess whether geodetic MDT variability is actual ocean signal or short spatial-scale errors in the geodetic observations.

4.5. Quasigeoid Performance

In order to assess the quasigeoid performance, we reconsider the data sources of the quasigeoid models. EGM2008 relies solely on GRACE data up to d/o 70 (∼285 km), and solely on terrestrial gravity information beyond d/o 120 (∼167 km) [*Pavlis et al*., 2012]. NMA2014 is purely based on terrestrial gravity data above d/o 140 (∼140 km), and GOCE DIR4 data below. The GOCE R5 models are dominated by GOCE data up to d/o ∼181 (∼110 km). This can be derived from the empirical relationship $n=1.45\times10^4/r$ between filter radius r and maximum SH degree n, as reported by *Zenner* [2006].

The GOCE R5 quasigeoids offer an improvement over NMA2014. This corresponds to our findings from GNSS/leveling (section 2.1.1). Considering the filter length, the improvement is related to the spectral band between d/o 140 and 180. On average, however, geodetic MDTs based on EGM2008 outperform the NMA2014-based quasigeoids. This contrasts the fact that EGM2008 performs worst in comparison with GNSS/leveling. This can be explained by the different quality of terrestrial gravity data over land and ocean. Undetected systematics in shipborne gravity may degrade the quality of the NMA2014-related quasigeoids over ocean, while EGM2008, which heavily relies on altimetry-derived gravity, is less affected. However, we cannot rule out the possibility that the dependence of EGM2008 on altimetry-derived gravity eliminates short-scale MDT signal in the geodetic MDT. Consequently, EGM2008-based geodetic MDTs are more similar to the smooth ocean MDTs, leading to smaller standard deviations of differences.

5. Conclusions

Returning to the goals of this work, we observe that along the Norwegian coast, geodetic and ocean MDTs agree on the ∼3–7 cm level at the tide gauges, and on the ∼5–11 cm level at the altimetry sites. In the Norwegian coastal area covered in this work, we quantify the ocean MDTs to contribute to the total error budget by 2–5 cm, while satellite altimetry and quasigeoid models contribute by less than 7 cm, respectively 4 cm. From the Taylor diagram intercomparison at the altimetry sites, we observe that geodetic MDTs based on both pointwise and gridded altimetry correlate with MDT_{Nemo12} on a similar level as the ocean models, suggesting a convergence of geodetic and ocean MDT approaches. The GOCE R5 quasigeoids offer an improvement over NMA2014. Over land, both models are superior to EGM2008, while the latter performs best over ocean areas. The dedicated coastal altimetry products generally do not offer an improvement over the conventional products they are based on. Pointwise monomission altimetry products give results comparable with the multimission DTU13MSS grid on the ∼5 cm level. Lacking ellipsoidal heights of MSL directly observed by GNSS, our tide-gauge geodetic MDT estimates rely on different height systems. For most sites, better results are obtained when using the new height system, NN2000. However, we stress the

importance of directly observing ellipsoidal heights of MSL at tide gauges by GNSS, thus ruling out possible distortions from leveling and quasigeoid errors.

Acknowledgments

We would like to thank O. C. D. Omang at the Norwegian Mapping Authority, for providing a set of GNSS/leveling points, the NMA2014 regional quasigeoid model for Norway, as well as valuable information regarding its determination. We further appreciate helpful comments from P. L. Woodworth at the National Oceanography Centre during the preparation of this paper. Thanks also go to C. W. Hughes at the National Oceanography Centre, for providing a suite of numerical ocean models. Taylor diagrams were created using G. Maze's MATLAB® script, at http://www.mathworks.com/matlabcentral/fileexchange/20559-taylor-diagram. Figure 1 was created using the M_Map package (http://www.eos.ubc.ca/~rich/map.html), with coastlines and political boundaries from the National Oceanic and Atmospheric Administration (http://www.ngdc.noaa.gov/mgg/shorelines/gshhs.html) and Natural Earth (http://www.naturalearthdata.com), respectively. The GGMs are available through the International Centre for Global Earth Models (ICGEM), at http://icgem.gfz-potsdam.de, and ACE2 is available at http://tethys.eaprs.cse.dmu.ac.uk/ACE2. Data used to produce Figures 2–5 and Tables 7–8 are available in the supporting information Tables S1 and S2. We further acknowledge the open data policies of the PSMSL, the Technical University of Denmark, the European Space Agency, the AVISO portal of CNES and CTOH, and MET Norway. This work is part of the Norwegian University of Life Science's GOCODYN project, supported by the Norwegian Research Council under project number 231017. Finally, we would like to thank Don Chambers and two anonymous reviewers for helpful comments that greatly improved the manuscript.

References

Ågren, J., and R. Svensson (2007), Postglacial land uplift model and system definition for the new Swedish height system RH2000, in *Reports in Geodesy and Geographical Information Systems*, 123 pp., Lantmäteriet, Gävle, Sweden.

Albertella, A., R. Savcenko, T. Janjić, R. Rummel, W. Bosch, and J. Schröter (2012), High resolution dynamic ocean topography in the Southern Ocean from GOCE, *Geophys. J. Int.*, *190*, 922–930, doi:10.1111/j.1365-246X.2012.05531.x.

Andersen, O. B., and P. Knudsen (2009), DNSC08 mean sea surface and mean dynamic topography models, *J. Geophys. Res.*, *114*, C11001, doi:10.1029/2008JC005179.

Andersen, O. B., L. Stenseng, and P. Knudsen (2013), The DTU13 global mean sea surface from 20 years of satellite altimetry, paper presented at the Ocean Surface Topography Science Team Meeting, Joint Office For Science Support (JOSS), Boulder, Colo., 8–11 Oct.

Baart, F., P. H. A. J. M. van Gelder, J. de Ronde, M. van Koningsveld, and B. Wouters (2012), The effect of the 18.6-year lunar nodal cycle on regional sea-level rise estimates, *J. Coastal Res.*, *28*(2), 511–516, doi:10.2112/JCOASTRES-D-11-00169.1.

Berry, P. A. M., R. G. Smith, and J. Benveniste (2010), ACE2: The New Global Digital Elevation Model, in *Gravity, Geoid and Earth Observation, Int. Assoc. Geod. Symp.*, vol. 135, edited by S. P. Mertikas, pp. 231–237, Springer, Berlin, doi:10.1007/978-3-642-10634-7_30.

Bingham, R. J., and K. Haines (2006), Mean dynamic topography: Intercomparisons and errors, *Philos. Trans. R. Soc. A*, *364*(1841), 903–916, doi:10.1098/rsta.2006.1745.

Bingham, R. J., P. Knudsen, O. Andersen, and R. Pail (2011), An initial estimate of the North Atlantic steady-state geostrophic circulation from GOCE, *Geophys. Res. Lett.*, *38*, L01606, doi:10.1029/2010GL045633.

Blaker, A. T., J. J.-M. Hirschi, G. McCarthy, B. Sinha, S. Taws, R. Marsh, A. Coward, and B. de Cuevas (2015), Historical analogues of the recent extreme minima observed in the Atlantic Meridional overturning circulation at 26°N, *Clim. Dyn.*, *44*, 457–473, doi:10.1007/s00382-014-2274-6.

Brockmann, J. M., N. Zehentner, E. Höck, R. Pail, I. Loth, T. Mayer-Gürr, and W.-D. Schuh (2014), EGM_TIM_RL05: An independent geoid with centimeter accuracy purely based on the GOCE mission, *Geophys. Res. Lett.*, *41*, 8089–8099, doi:10.1002/2014GL061904.

Bruinsma, S. L., C. Förste, O. Abrikosov, J.-C. Marty, M.-H. Rio, S. Mulet, and S. Bonvalot (2013), The new ESA satellite-only gravity field model via the direct approach, *Geophys. Res. Lett.*, *40*, 3607–3612, doi:10.1002/grl.50716.

Cartwright, D. E., and A. C. Edden (1973), Corrected tables of tidal harmonics, *Geophys. J. R. Astron. Soc.*, *23*(1), 45–73, doi:10.1111/j.1365-246X.1973.tb03420.x.

Cartwright, D. E., and R. J. Tayler (1971), New computations of the tide-generating potential, *Geophys. J. R. Astron. Soc.*, *33*(3), 253–264, doi:10.1111/j.1365-246X.1971.tb01803.x.

Denker, H. (2013), Regional gravity field modeling: Theory and practical results, in *Sciences of Geodesy – II*, edited by G. Xu, pp. 185–291, Springer, Berlin, doi:10.1007/978-3-642-28000-9_5.

Drinkwater, M. R., R. Floberghagen, R. Haagmans, D. Muzi, and A. Popescu (2003), GOCE: ESA's first Earth Explorer Core mission, in *Earth Gravity Field from Space — From Sensors to Earth Sciences, Space Sciences Series of ISSI*, edited by G. Beutler et al., pp. 419–432, Springer, Dordrecht, Netherlands, doi:10.1007/978-94-017-1333-7_36.

Ekman, M. (1989), Impacts of geodynamic phenomena on systems for height and gravity, *Bull. Geod.*, *63*, 281–296, doi:10.1007/BF02520477.

Featherstone, W. E. (2008), GNSS-based heighting in Australia: Current, emerging and future issues, *J. Spatial Sci.*, *53*(2), 115–133, doi:10.1080/14498596.2008.9635153.

Featherstone, W. E., and M. S. Filmer (2012), The north-south tilt in the Australian Height Datum is explained by the ocean's mean dynamic topography, *J. Geophys. Res.*, *117*, C08035, doi:10.1029/2012JC007974.

Filmer, M. S. (2014), Using models of the ocean's mean dynamic topography to identify errors in coastal geodetic levelling, *Mar. Geod.*, *37*, 47–64, doi:10.1080/01490419.2013.868383.

Forsberg, R., and W. Featherstone (1998), Geoids and cap sizes, in *Geodesy on the Move, Int. Assoc. Geod. Symp.*, vol. 119, edited by R. Forsberg et al., pp. 194–200, Springer, Berlin, doi:10.1007/978-3-642-72245-5_27.

Gommenginger, C., P. Thibaut, L. Fenoglio-Marc, G. Quartly, X. Deng, J. Gómez-Enri, P. Challenor, and Y. Gao (2011), Retracking altimeter waveforms near the coasts, in *Coastal Altimetry*, edited by S. Vignudelli et al., pp. 61–101, Springer, Berlin, doi:10.1007/978-3-642-12796-0_4.

Griesel, A., M. R. Mazloff, and S. T. Gille (2012), Mean dynamic topography in the Southern Ocean: Evaluating Antarctic Circumpolar Current transport, *J. Geophys. Res.*, *117*, C01020, doi:10.1029/2011JC007573.

Gruber, T. (2014), GOCE gravity field models—Overview and performance analysis, paper presented at the 5th International GOCE User Workshop, European Space Agency, Paris, 25–28 Nov., European Space Agency.

Haagmans, R., E. de Min, and M. von Gelderen (1993), Fast evaluation of convolution integrals on the sphere using 1D FFT, and a comparison with existing methods for Stokes's integral, *Manuscr. Geod.*, *18*, 227–241.

Haines, K., J. A. Johannessen, P. Knudsen, D. Lea, M.-H. Rio, L. Bertino, F. Davidson, and F. Hernandez (2011), An ocean modelling and assimilation guide to using GOCE geoid products, *Ocean Sci.*, *7*, 151–164, doi:10.5194/os-7-151-2011.

Higginson, S., K. R. Thompson, P. L. Woodworth, and C. W. Hughes (2015), The tilt of mean sea level along the east coast of North America, *Geophys. Res. Lett.*, 1471–1479, doi:10.1002/2015GL063186.

Hofmann-Wellenhof, B., and H. Moritz (2005), *Physical Geodesy*, Springer, Wien, Austria.

Hofmann-Wellenhof, B., H. Lichtenegger, and J. Collins (2001), *Global Positioning System: Theory and Practice*, Springer, Wien, Austria.

Holgate, S. J., A. Matthews, P. L. Woodworth, L. J. Rickards, M. E. Tamisiea, E. Bradshaw, P. R. Foden, K. M. Gordon, S. Jevrejeva, and J. Pugh (2013), New data systems and products at the Permanent Service for Mean Sea Level, *J. Coastal Res.*, *29*, 493–504, doi:10.2112/JCOASTRES-D-12-00175.1.

Holt, J. T., and I. D. James (2001), An s coordinate density evolving model of the northwest European continental shelf: 1. Model description and density structure, *J. Geophys. Res.*, *106*, 14,015–14,034, doi:10.1029/2000JC000304.

Hughes, C. W., R. J. Bingham, V. Roussenov, J. Williams, and P. L. Woodworth (2015), The effect of Mediterranean exchange flow on European time mean sea level, *Geophys. Res. Lett.*, *42*, 466–474, doi:10.1002/2014GL062654.

Jayne, S. R. (2006), Circulation of the North Atlantic Ocean from altimetry and the Gravity Recovery and Climate Experiment geoid, *J. Geophys. Res.*, *111*, C03005, doi:10.1029/2005JC003128.

Jekeli, C. (1981), Alternative methods to smooth the Earth's gravity field, *Tech. Rep. 327*, Dept. of Geod. Sci. and Surv., Ohio State Univ., Columbus.

Johannessen, J. A., et al. (2014), Toward improved estimation of the dynamic topography and ocean circulation in the high latitude and Arctic ocean: The importance of GOCE, *Surv. Geophys.*, *35*, 661–679, doi:10.1007/s10712-013-9270-y.

Kierulf, H. P., M. Ouassou, and M. J. R. Simpson (2013), A continuous velocity field for Norway, *J. Geod.*, *87*, 337–349, doi:10.1007/s00190-012-0603-2.
Lysaker, D. I., O. C. D. Omang, B. R. Pettersen, and D. Solheim (2007), Quasigeoid evaluation with improved levelled height data for Norway, *J. Geod.*, *81*, 617–627, doi:10.1007/s00190-006-0129-6.
Madec, G. (2008), *NEMO ocean engine, Note du Pole de modélisation*, vol. 27, pp. 1288–1619, Inst. Pierre-Simon Laplace, Paris, France.
Marsh, R., B. A. de Cuevas, A. C. Coward, J. Jacquin, J. J.-M. Hirschi, Y. Aksenov, A. J. G. Nurser, and S. A. Josey (2009), Recent changes in the North Atlantic circulation simulated with eddy-permitting and eddy-resolving ocean models, *Ocean Modell.*, *28*, 226–239, doi:10.1016/j.ocemod.2009.02.007.
Marshall J., C. Hill, L. Perelman, and A. Adcroft (1997a), Hydrostatic, quasi-hydrostatic, and nonhydrostatic ocean modelling, *J. Geophys. Res.*, *102*, 5733–5752, doi:10.1029/96JC02776.
Marshall J., A. Adcroft, C. Hill, L. Perelman, and C. Heisey (1997b), A finite-volume, incompressible Navier Stokes model for studies of the ocean on parallel computers, *J. Geophys. Res.*, *102*, 5753–5766, doi:10.1029/96JC02775.
Mercier, F., et al. (2008), Improved Jason-2 altimetry products for coastal zones and continental waters (PISTACH project), paper presented at the Ocean Surface Topography Science Team Meeting, National Aeronautics and Space Administration, National Oceanic and Atmospheric Administration, Centre national d'études spatiales, European Space Agency, Nice, 10–15 Nov, Nice, France.
Mork, K. A., and Ø. Skagseth (2010), A quantitative description of the Norwegian Atlantic Current by combining altimetry and hydrography, *Ocean Sci.*, *6*, 901–911, doi:10.5194/os-6-901-2010.
Mysen, E. (2014), On the computation of reliable formal uncertainties in the densification of GPS-levelling networks by least-squares collocation, *J. Geod.*, *88*, 917–926, doi:10.1007/s00190-014-0732-x.
Ollivier, A., and M. Guibbaud (2012), Envisat RA2/MWR reprocessing impact on ocean data, technical report ESA CLS.DOS/NT/12.064, Collect. Localisation Satell., Ramonville St-Agne, France.
Omang, O. C. D., and R. Forsberg (2002), The northern European geoid: A case study on long-wavelength geoid errors, *J. Geod.*, *76*, 369–380, doi:10.1007/s00190-002-0261-x.
Pavlis, N. K., S. A. Holmes, S. C. Kenyon, and J. K. Factor (2012), The development and evaluation of the Earth Gravitational Model 2008 (EGM2008), *J. Geophys. Res.*, *117*, B04406, doi:10.1029/2011JB008916.
Petit, G., and B. Luzum (eds.) (2010), IERS Conventions (2010), *IERS Tech. Note 36*, 179 pp., Verlag des Bundesamts für Kartographie und Geod., Frankfurt am Main, Germany.
Prandi, P., M. Ablain, A. Cazenave, and N. Picot (2012), A new estimation of mean sea level in the Arctic Ocean from satellite altimetry, *Mar. Geod.*, *35*(S1), 61–82, doi:10.1080/01490419.2012.718222.
Pugh, D., and P. L. Woodworth (2014), *Sea-Level Science: Understanding Tides, Surges, Tsunamis and Mean Sea-Level Changes*, Cambridge Univ. Press, Cambridge, U. K.
Ray, R. D., G. D. Egbert, and S. Y. Erofeeva (2011), Tide predictions in shelf and coastal waters: Status and prospects, in *Coastal Altimetry*, edited by S. Vignudelli et al., pp. 191–216, Springer, Berlin, doi:10.1007/978-3-642-12796-0_8.
Rhines, P., S. Häkkinen, and S. A. Josey (2008), Is oceanic heat transport significant in the climate system?, in *Arctic-Subarctic Ocean Fluxes*, edited by R. R. Dickson et al., pp. 87–109, Springer, Dordrecht, Netherlands, doi:10.1007/978-1-4020-6774-7_5.
Roblou, L., J. Lamouroux, J. Bouffard, F. Lyard, M. Le Hénaff, A. Lombard, P. Marsalaix, P. De Mey, and F. Birol (2011), Post-processing altimeter data toward coastal applications and integration into coastal models, in *Coastal Altimetry*, edited by S. Vignudelli et al., pp. 217–246, Springer, Berlin, doi:10.1007/978-3-642-12796-0_9.
Rothacher, M. (2002), Estimation of station heights with GPS, in *Vertical Reference Systems*, edited by H. Drewes et al., pp. 81–90, Springer, Berlin, doi:10.1007/978-3-662-04683-8_17.
Rülke, A., G. Liebsch, M. Sacher, U. Schäfer, U. Schirmer, and J. Ihde (2012), Unification of European height system realizations, *J. Geod. Sci.*, *2*, 343–354, doi:10.2478/v10156-012-0004-8.
Rummel, R. (2012), Height unification using GOCE, *J. Geod. Sci.*, *2*, 355–362, doi:10.2478/v10156-011-0047-2.
Sideris, M. G. (2013), Geoid Determination by FFT Techniques, in *Geoid Determination, Lecture Notes in Earth System Sciences*, edited by F. Sansò and M. G. Sideris, pp. 453–516, Springer, Berlin, doi:10.1007/978-3-540-74700-0_10.
Skagseth, Ø., K. F. Drinkwater, and E. Terrile (2011), Wind- and buoyancy-induced transport of the Norwegian Coastal Current in the Barents Sea, *J. Geophys. Res.*, *116*, C08007, doi:10.1029/2011JC006996.
Smith, D. M., and J. M. Murphy (2007), An objective ocean temperature and salinity analysis using covariances from a global climate model, *J. Geophys. Res.*, *112*, C02022, doi:10.1029/2005JC003172.
Solheim, D. (2000), New height reference surfaces for Norway, in *Report on the Symposium of the IAG Subcommission for Europe (EUREF) in Tromsø*, edited by J. A. Torres and H. Hornik, pp. 154–158, Verlag der Bayer. Akad. der Wiss., Munich, Germany, 22–24 June.
Soussi, B., M. Roca, D. Cotton, and P. Féménias (2009), *Envisat RA-2/MWR Level 2 User Manual*, version 1.3, 162 pp., European Space Agency, Noordwijk, Netherlands.
Šprlák, M., C. Gerlach, and B. R. Pettersen (2015), Validation of GOCE global gravitational field models in Norway, *Newton's Bull.*, *5*, 3–12, ISSN 1810-8555.
Taylor, K. (2001), Summarizing multiple aspects of model performance in a single diagram, *J. Geophys. Res.*, *106*, 7183–7192, doi:10.1029/2000JD900719.
Thompson, K. R., J. Huang, M. Véronneau, D. G. Wright, and Y. Lu (2009), Mean surface topography of the northwest Atlantic: Comparison of estimates based on satellite, terrestrial gravity, and oceanographic observations, *J. Geophys. Res.*, *114*, C07015, doi:10.1029/2008JC004859.
Vestøl, O. (2006), Determination of Postglacial Land Uplift in Fennoscandia from Leveling, Tide-gauges and Continuous GPS Stations using Least Squares Collocation, *J. Geod.*, *80*, 248–258, doi:10.1007/s00190-006-0063-7.
Wahr, J. M. (1985), Deformation induced by polar motion, *J. Geophys. Res.*, *90*, 9363–9368, doi:10.1029/JB090iB11p09363.
Webb, D. J., A. C. Coward, B. A. de Cuevas, and C. S. Gwilliam (1997), A multiprocessor ocean general circulation model using message passing, *J. Atmos. Oceanic Technol.*, *14*, 175–182, doi:10.1175/1520-0426(1997)014 < 0175:AMOGCM>2.0.CO;2.
Wong, L., and R. Gore (1969), Accuracy of geoid heights from modified Stokes kernels, *Geophys. J. R. Astron. Soc.*, *18*, 81–91.
Woodworth, P. L. (2012), A note on the nodal tide in sea level records, *J. Coastal Res.*, *28*(2), 316–323, doi:10.2112/JCOASTRES-D-11A-00023.1.
Woodworth, P. L., C. Hughes, R. J. Bingham, and T. Gruber (2012), Towards worldwide height system unification using ocean information, *J. Geod. Sci.*, *2*, 302–318, doi:10.2478/v10156-012-0004-8.
Woodworth, P. L., M. Gravelle, M. Marcos, G. Wöppelmann, and C. W. Hughes (2015), The status of measurement of the Mediterranean mean dynamic topography by geodetic techniques, *J. Geod.*, *89*, 1–17, doi:10.1007/s00190-015-0817-1.
Wunsch, C., and D. Stammer (1997), Atmospheric loading and the oceanic "inverted barometer" effect, *Rev. Geophys.*, *35*, 79–107, doi:10.1029/96RG030337.
Zenner, L. (2006), Zeitliche Schwerefeldvariationen aus GRACE und Hydrologiemodellen, diploma thesis, Inst. für Astron. und Phys. Geod., Tech. Univ. München, Munich, Germany.